Electronic Supporting Information

Superior bifunctional cobalt/nitrogen-codoped carbon nanosheet arrays on copper foam enable stable energy-saving hydrogen production accompanied with glucose upgrading

Yu Xin,[ab] Fengliang Wang,[ab] Liyu Chen,[ab] Yingwei Li[ab] and Kui Shen*[ab]*

[a] *State Key Laboratory of Pulp and Paper Engineering, School of Chemistry and Chemical Engineering, South China University of Technology, Guangzhou 510640, China.*

[b] *Key Laboratory of Fuel Cell Technology of Guangdong Province, School of Chemistry and Chemical Engineering, South China University of Technology, Guangzhou 510640, China*

* Corresponding authors: Y. Li and K. Shen, E-mail: liyw@scut.edu.cn; cekshen@scut.edu.cn

This file includes supplementary Figures S1-S36, and Table S1-S4.

Supplementary Figures

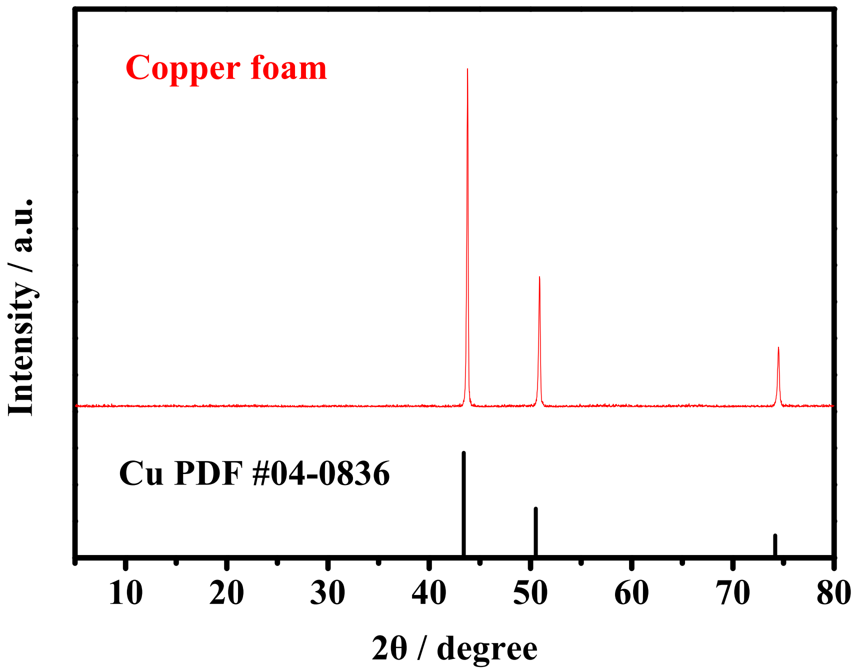

Figure S1. The XRD pattern of copper foam (CF) and the standard line of Cu.

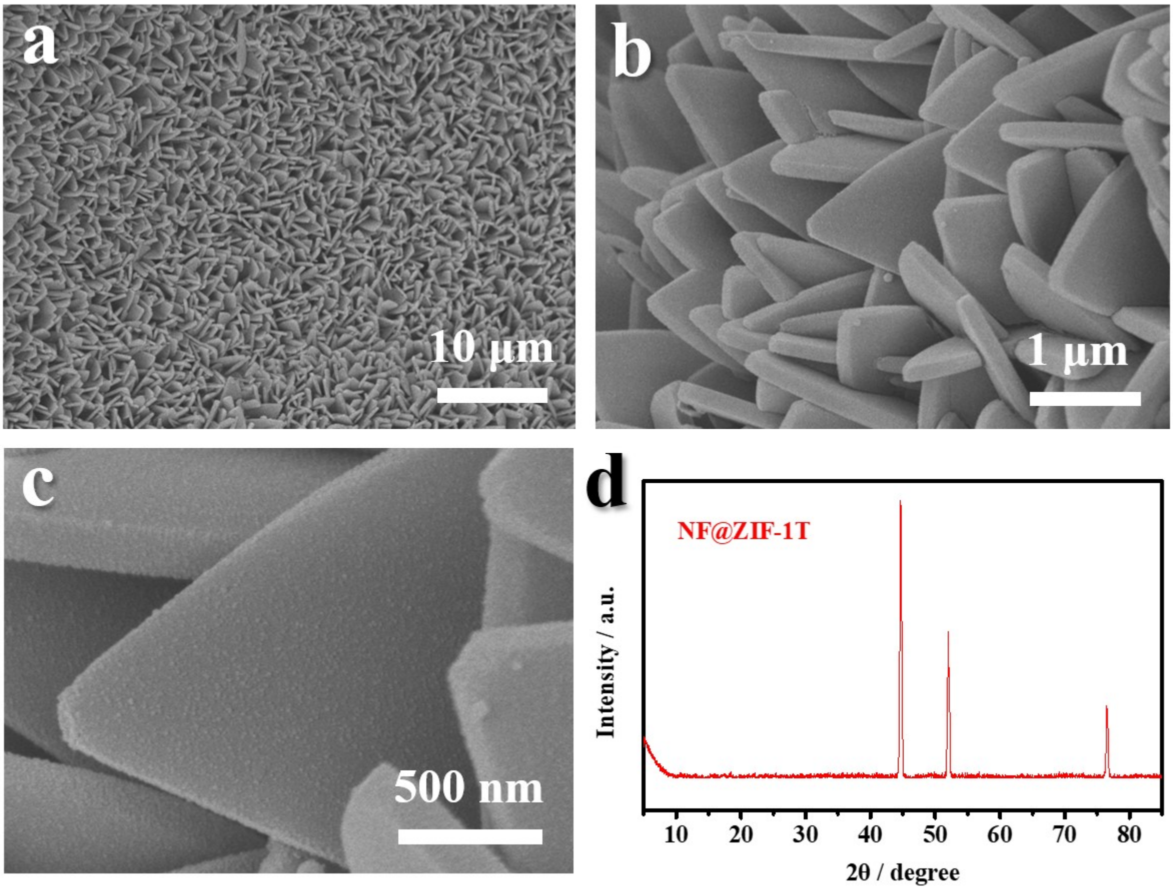

Figure S2. Characterization of NF@ZIF-1T. a-c) Low- and high-magnification SEM images, and d) XRD pattern.

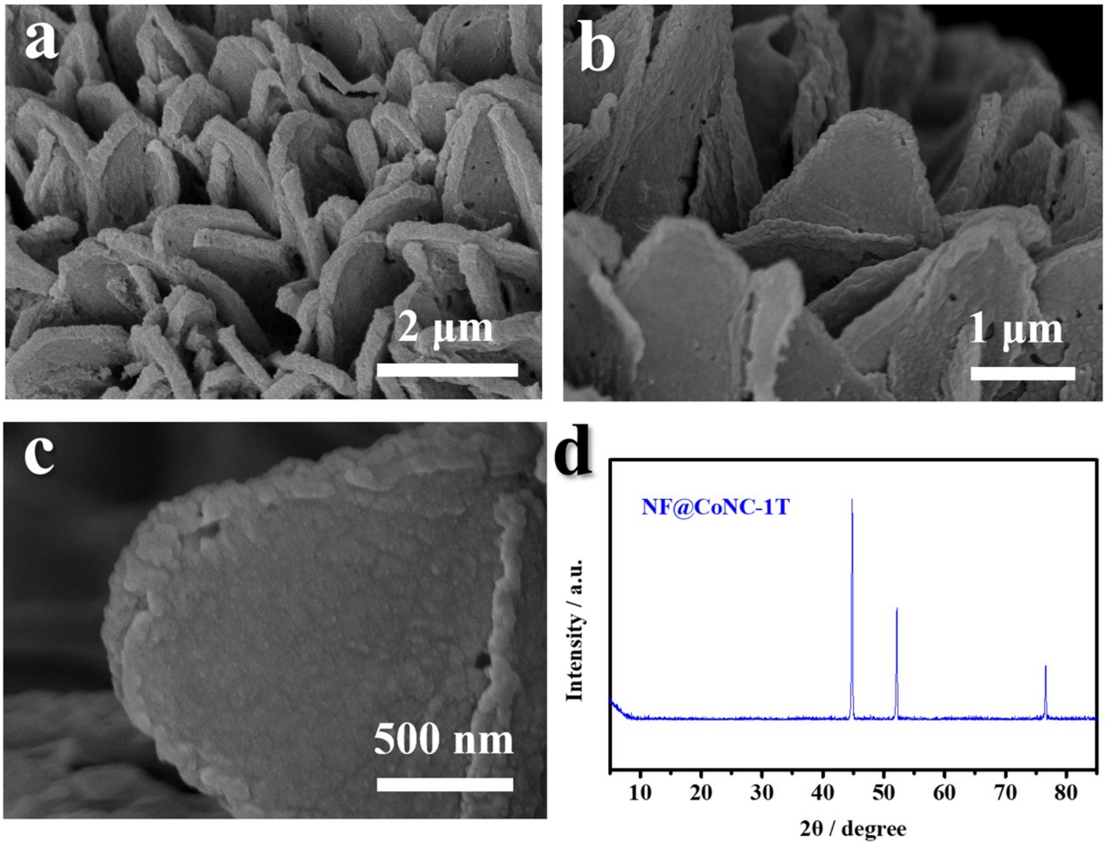

Figure S3. Characterization of NF@CoNC-1T. a-c) Low- and high-magnification SEM images, and d) XRD pattern.

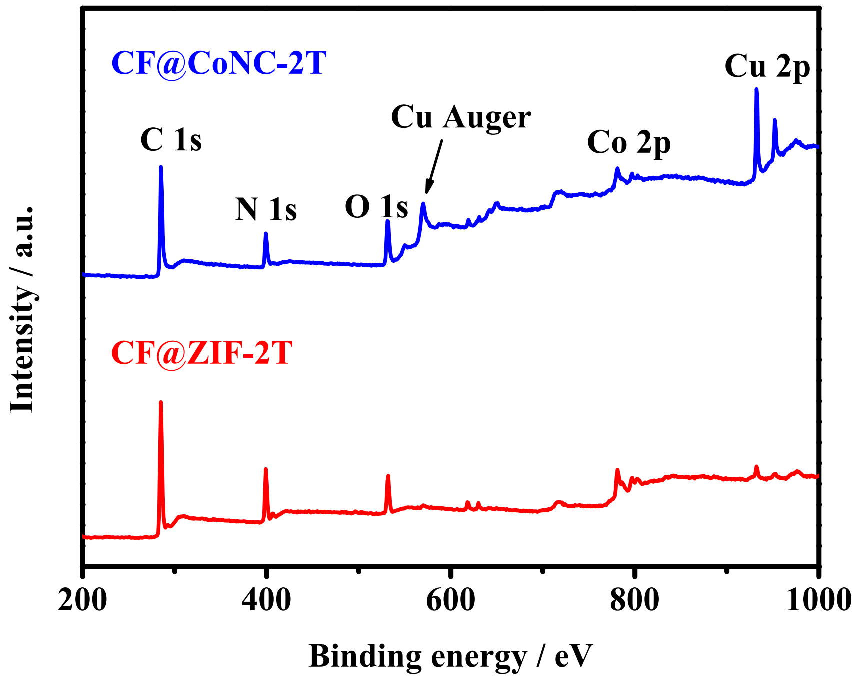

Figure S4. The full XPS survey spectra of CF@ZIF-2T and CF@CoNC-2T.

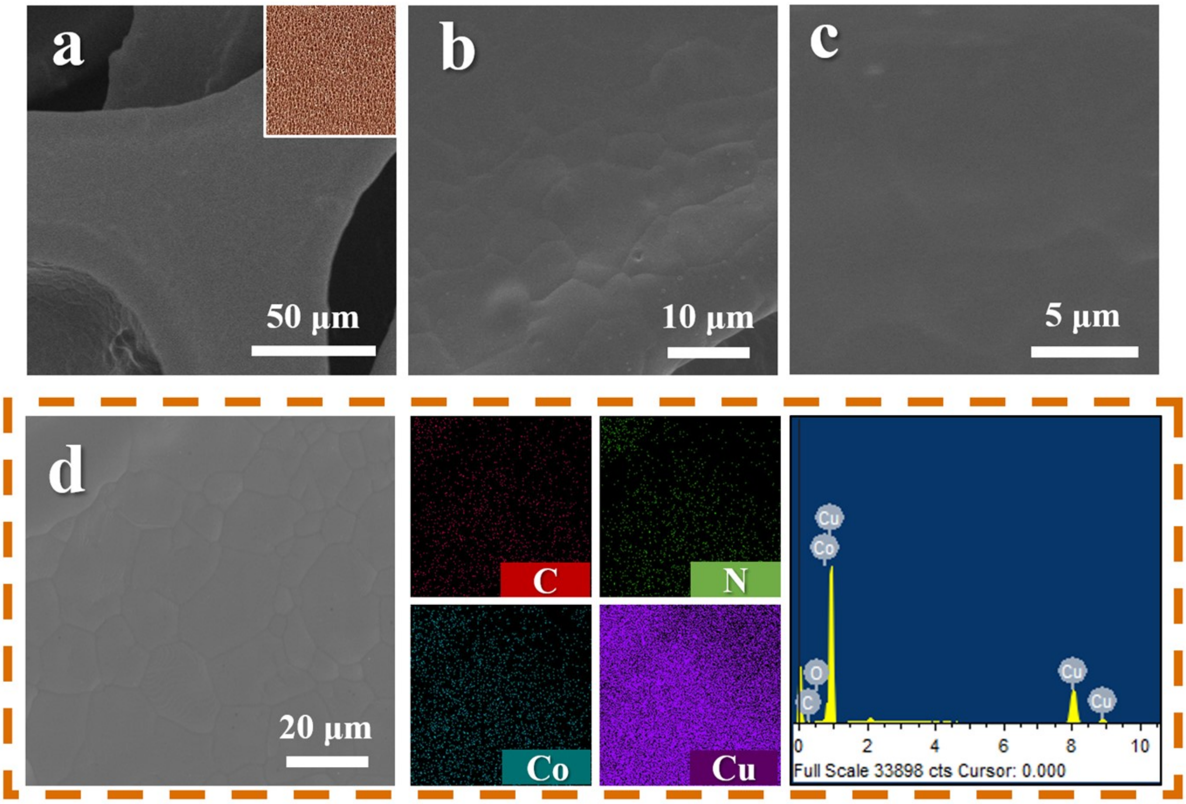

Figure S5. Characterization of copper foam (CF). (a-c) Low- and high-magnification SEM images of CF after spraying a conductive Au coating. (d) SEM image of CF without a conductive coating and its corresponding EDS mapping images and element spectrum. The inset in (a) is the optical photograph of CF.

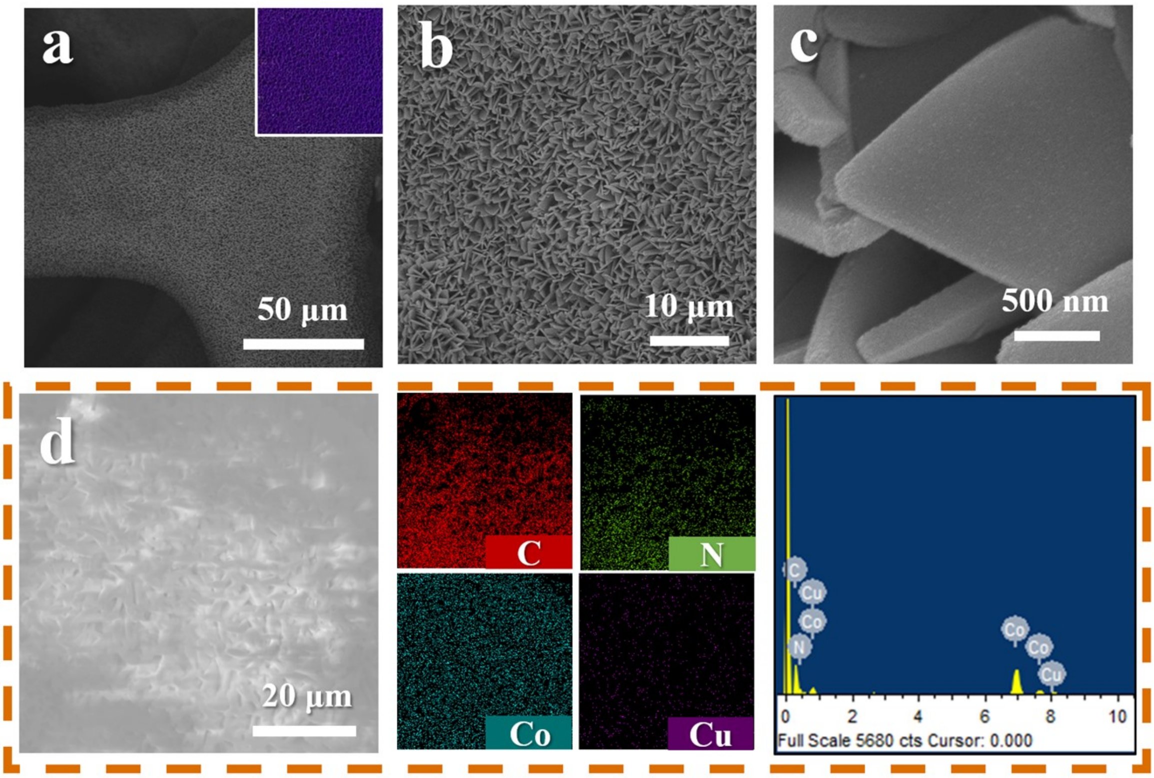

Figure S6. Characterization of CF@ZIF-1T. (a-c) Low- and high-magnification SEM images of CF@ZIF-1T after spraying a conductive Au coating. (d) SEM image of CF@ZIF-1T without a conductive coating and its corresponding EDS mapping images and element spectrum. The inset in (a) is the optical photograph of CF@ZIF-1T.

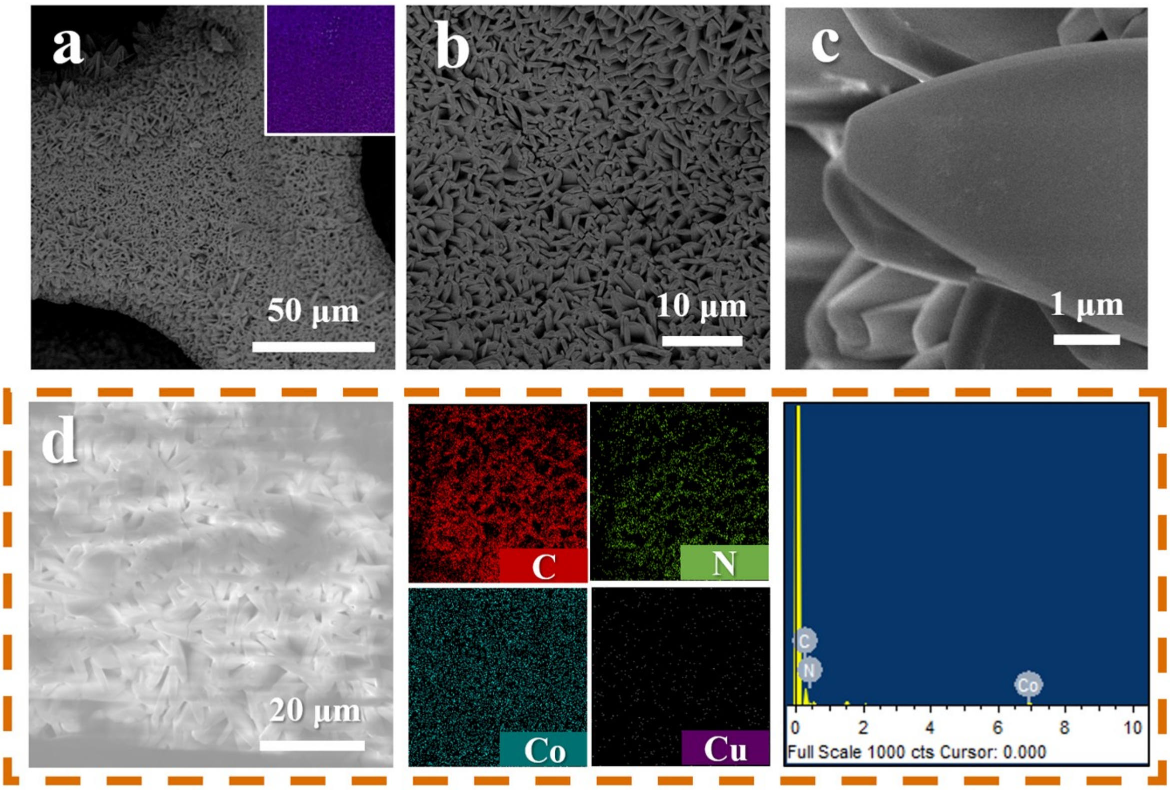

Figure S7. Characterization of CF@ZIF-2T. (a-c) Low- and high-magnification SEM images of CF@ZIF-2T after spraying a conductive Au coating. (d) SEM image of CF@ZIF-2T without a conductive coating and its corresponding EDS mapping images and element spectrum. The inset in (a) is the optical photograph of CF@ZIF-2T.

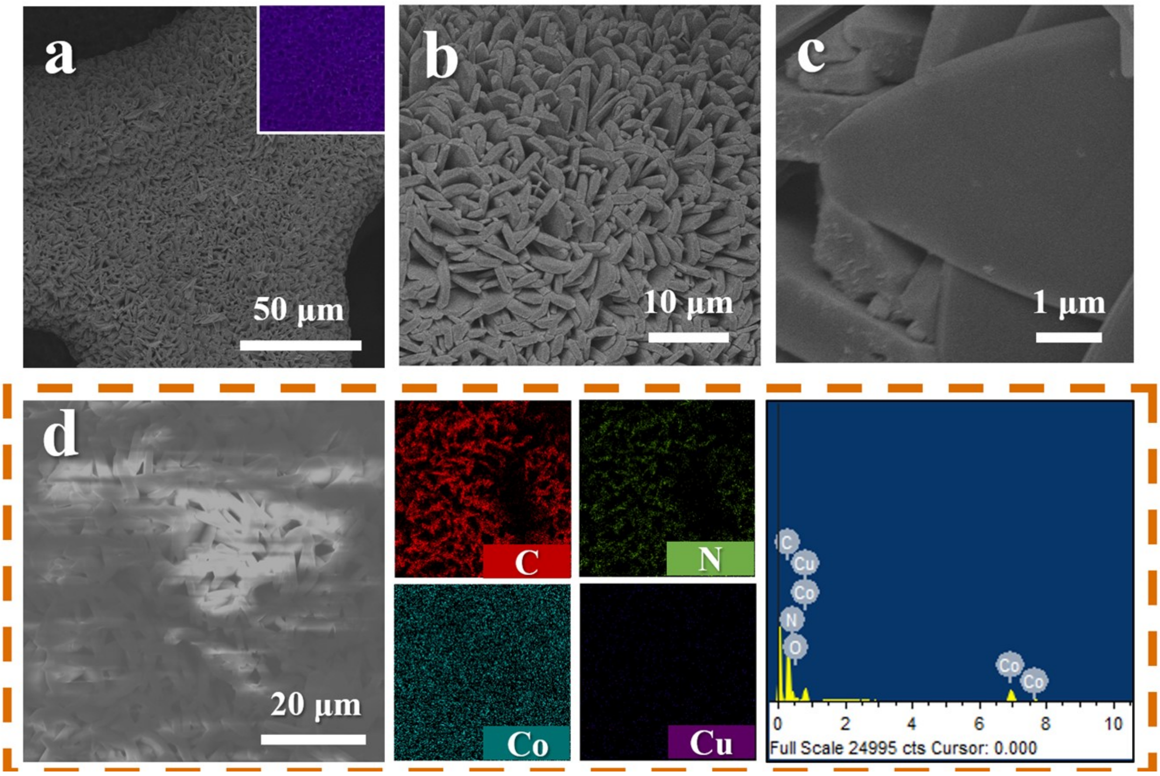

Figure S8. Characterization of CF@ZIF-3T. (a-c) Low- and high-magnification SEM images of CF@ZIF-3T after spraying a conductive Au coating. (d) SEM image of CF@ZIF-3T without a conductive coating and its corresponding EDS mapping images and element spectrum. The inset in (a) is the optical photograph of CF@ZIF-3T.

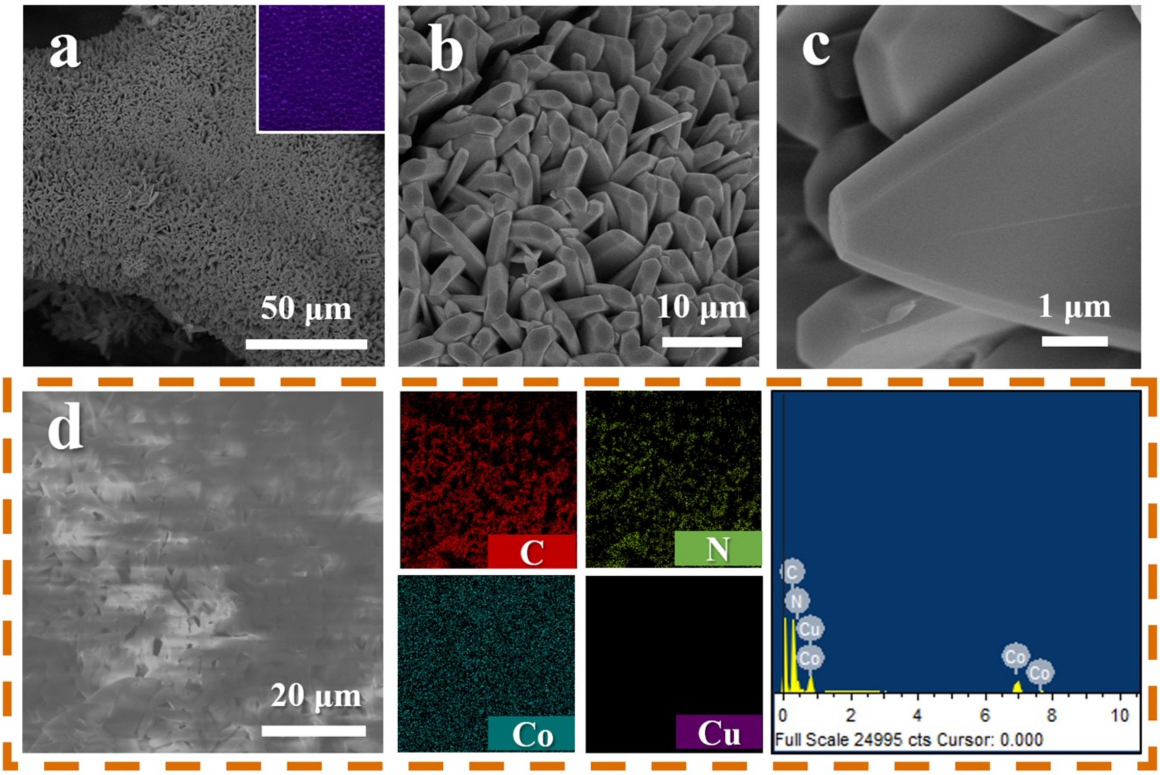

Figure S9. Characterization of CF@ZIF-4T. (a-c) Low- and high-magnification SEM images of CF@ZIF-4T after spraying a conductive Au coating. (d) SEM image of CF@ZIF-4T without a conductive coating and its corresponding EDS mapping images and element spectrum. The inset in (a) is the optical photograph of CF@ZIF-4T.

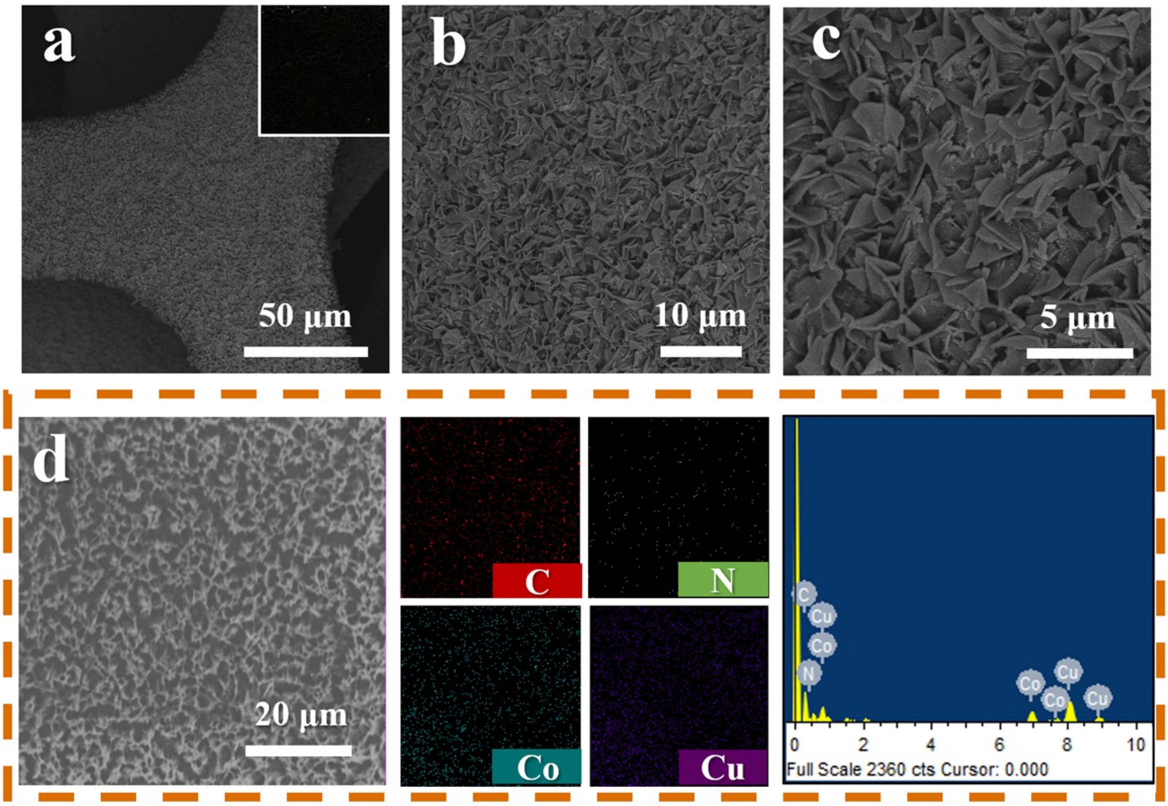

Figure S10. Characterization of CF@CoNC-1T. (a-c) Low- and high-magnification SEM images of CF@CoNC-1T after spraying a conductive Au coating. (d) SEM image of CF@CoNC-1T without a conductive coating and its corresponding EDS mapping images and element spectrum. The inset in (a) is the optical photograph of CF@CoNC-1T.

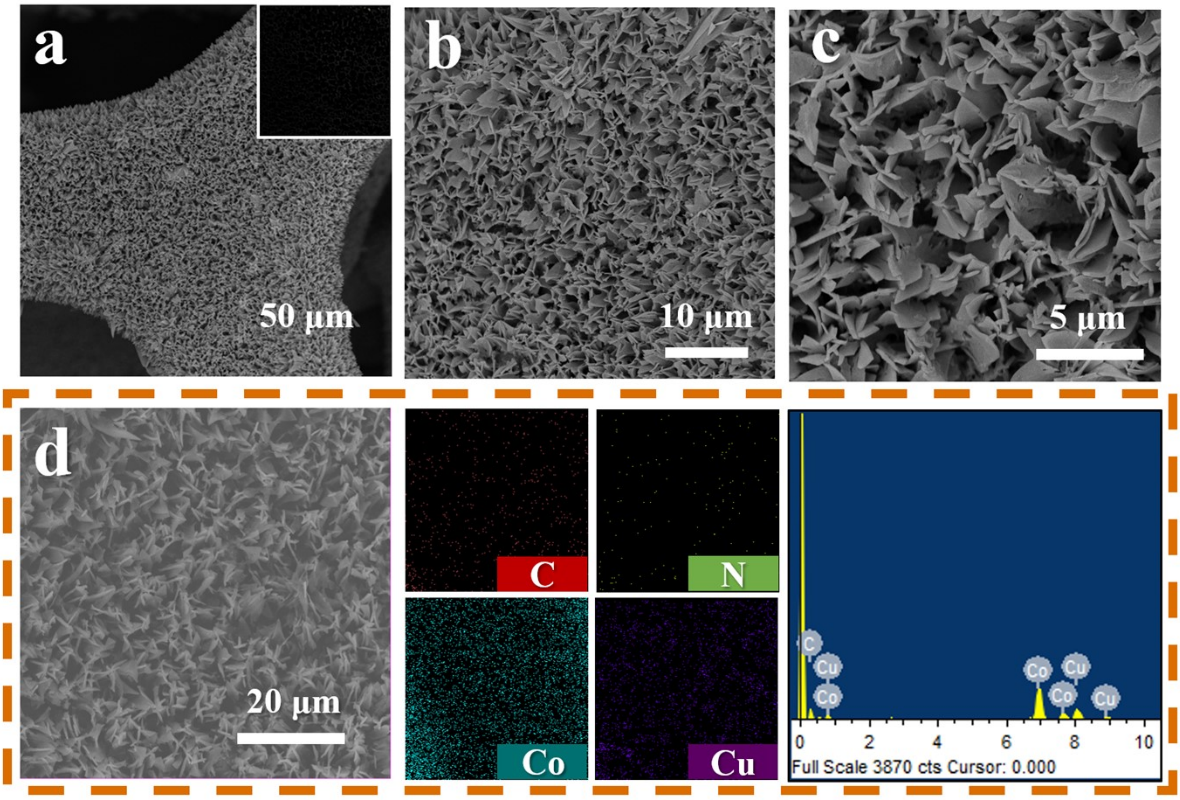

Figure S11. Characterization of CF@CoNC-2T. (a-c) Low- and high-magnification SEM images of CF@CoNC-2T after spraying a conductive Au coating. (d) SEM image of CF@CoNC-2T without a conductive coating and its corresponding EDS mapping images and element spectrum. The inset in (a) is the optical photograph of CF@CoNC-2T.

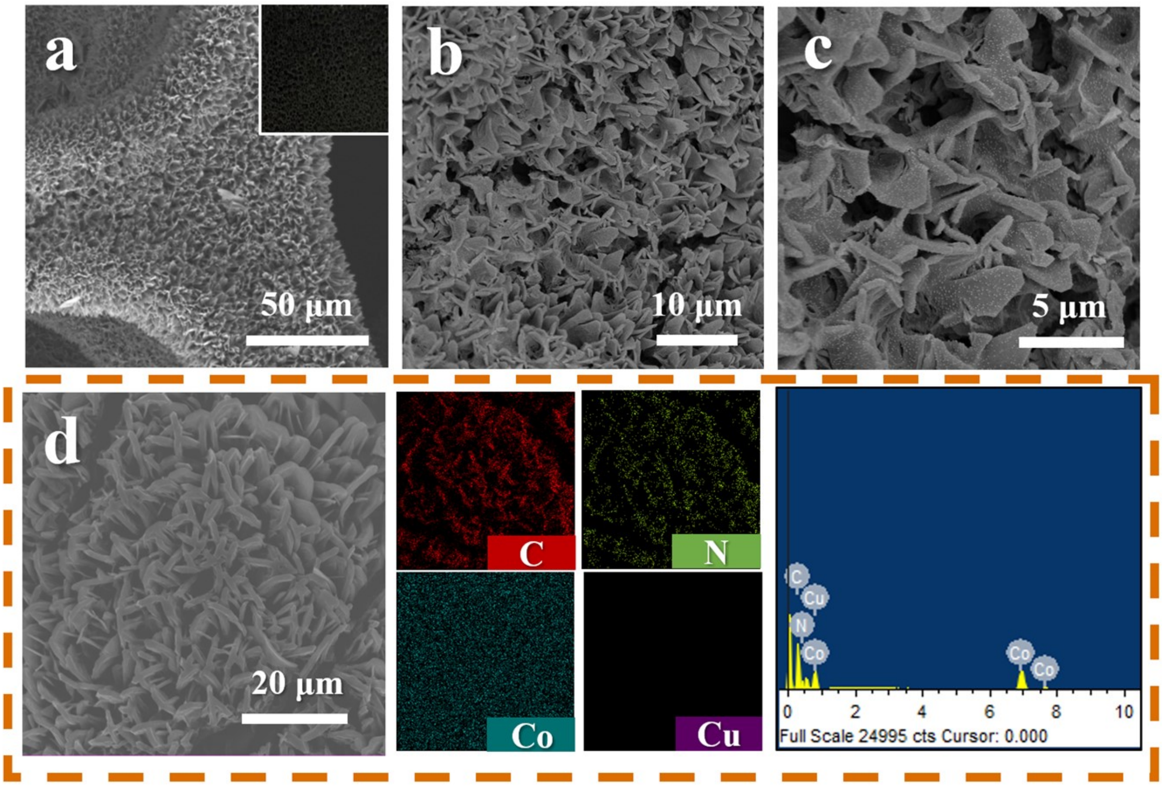

Figure S12. Characterization of CF@CoNC-3T. (a-c) Low- and high-magnification SEM images of CF@CoNC-3T after spraying a conductive Au coating. (d) SEM image of CF@CoNC-3T without a conductive coating and its corresponding EDS mapping images and element spectrum. The inset in (a) is the optical photograph of CF@CoNC-3T.

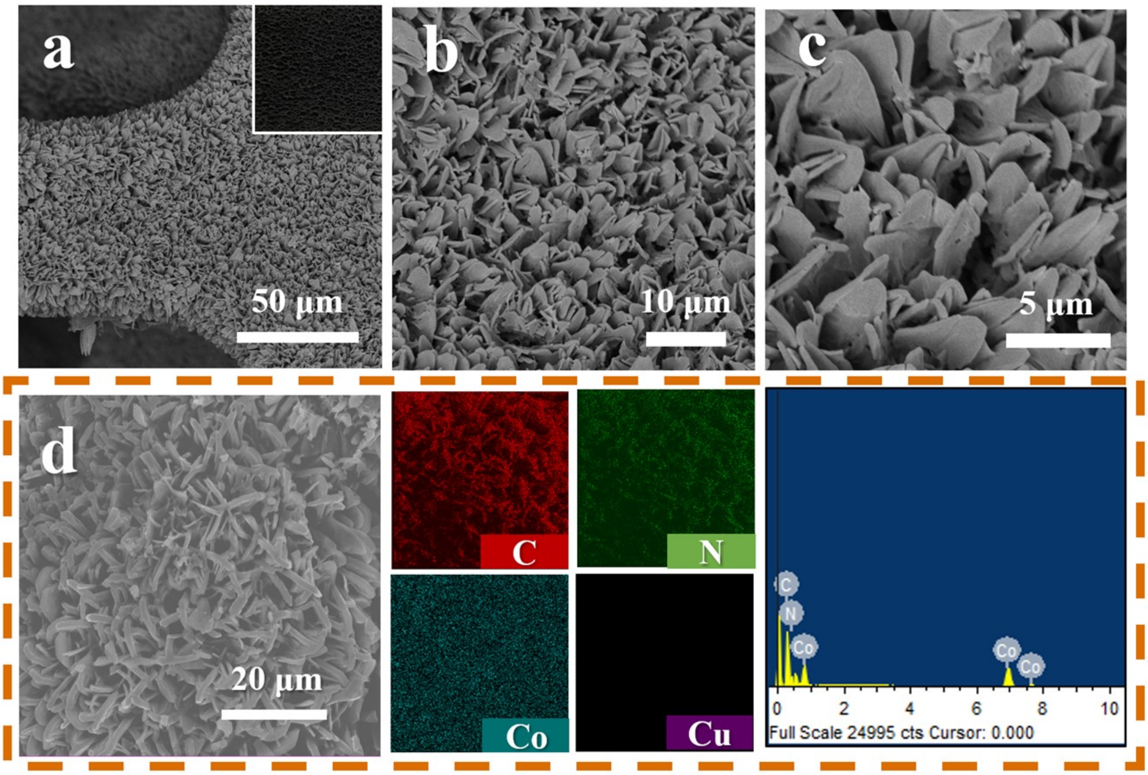

Figure S13. Characterization of CF@CoNC-4T. (a-c) Low- and high-magnification SEM images of CF@CoNC-4T after spraying a conductive Au coating. (d) SEM image of CF@CoNC-4T without a conductive coating and its corresponding EDS mapping images and element spectrum. The inset in (a) is the optical photograph of CF@CoNC-4T.

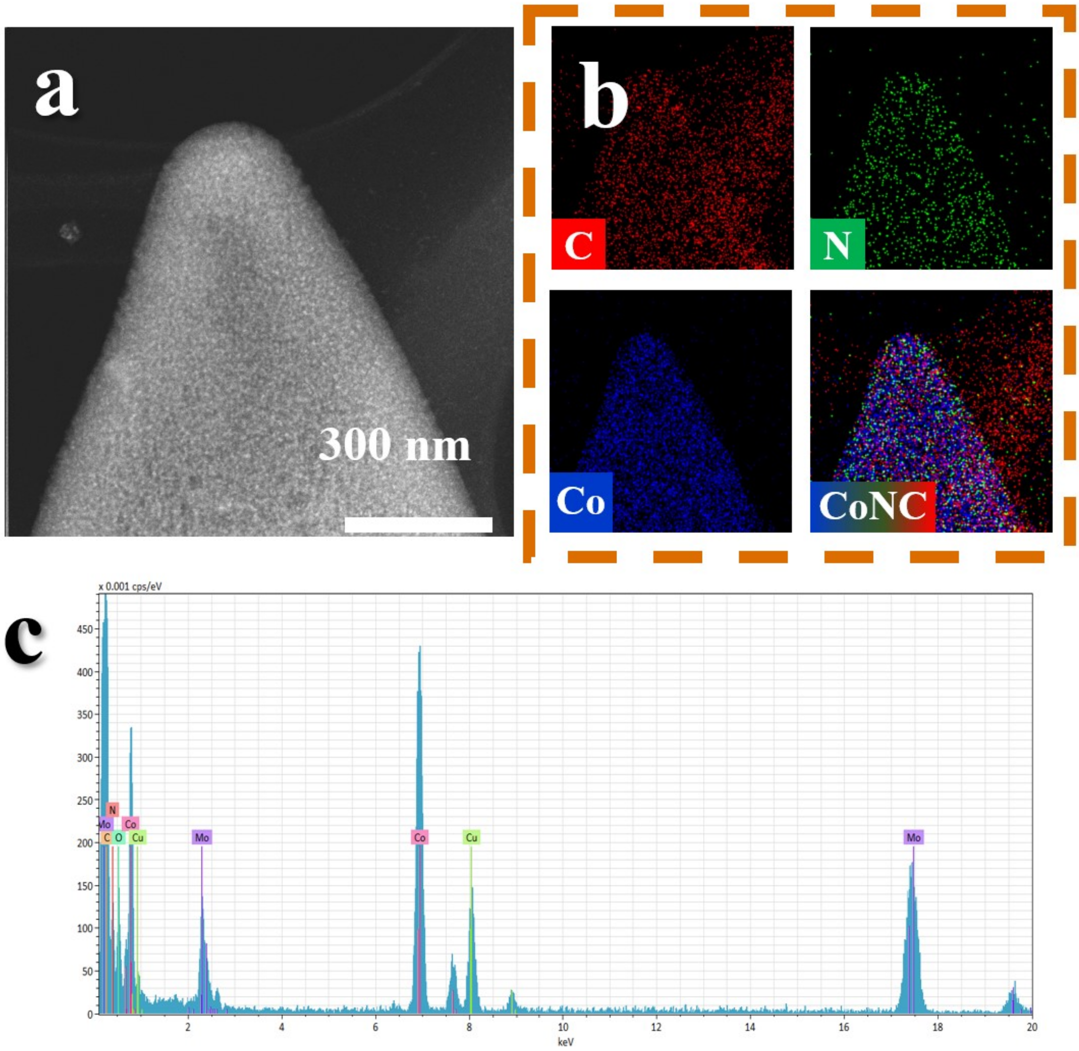

Figure S14. (a) HAADF-STEM and (b) EDS mapping images and (c) the corresponding elemental spectrum of CF@CoNC-1T.

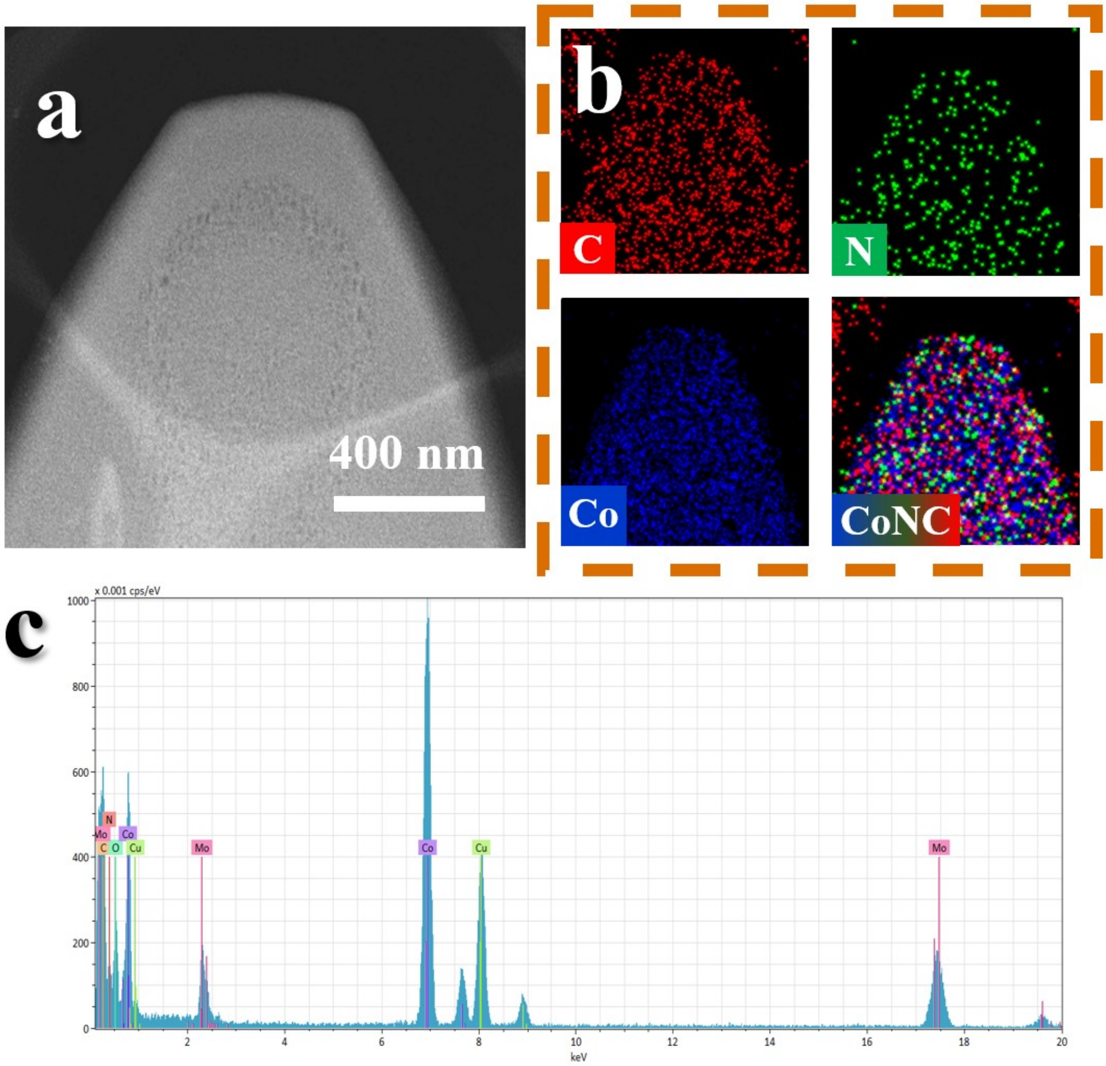

Figure S15. (a) HAADF-STEM and (b) EDS mapping images and (c) the corresponding elemental spectrum of CF@CoNC-2T.

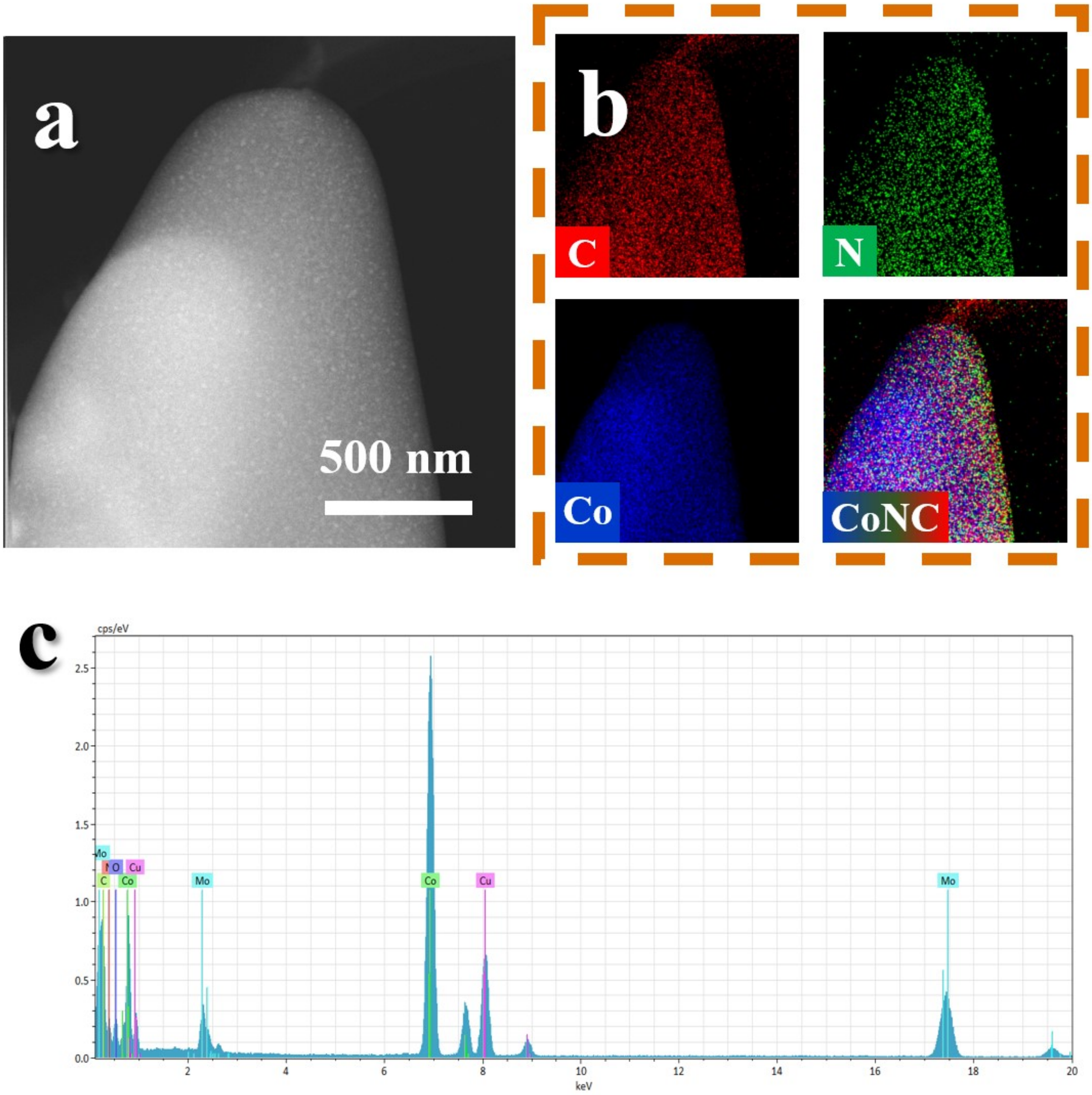

Figure S16. (a) HAADF-STEM and (b) EDS mapping images and (c) the corresponding elemental spectrum of CF@CoNC-3T.

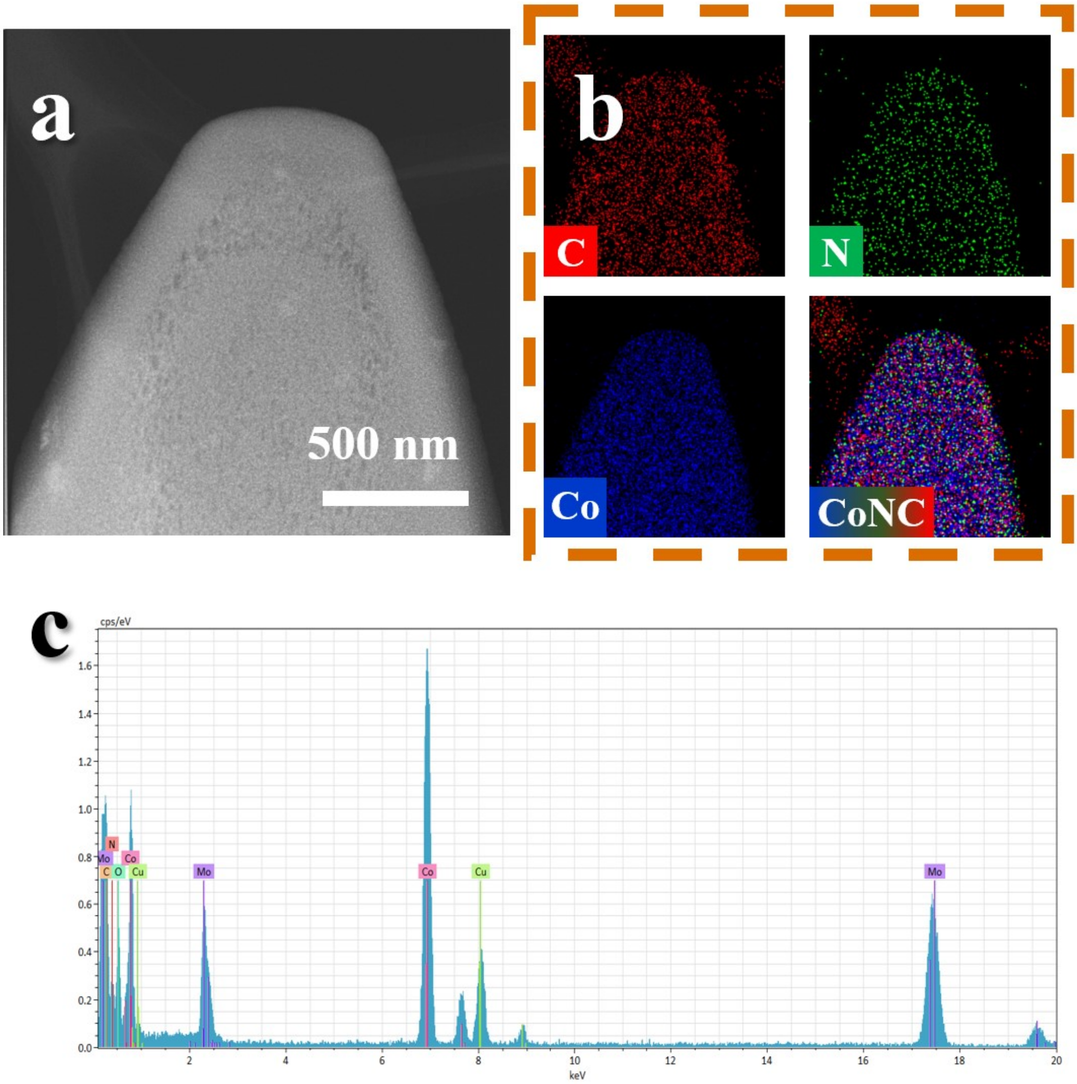

Figure S17. (a) HAADF-STEM and b) EDS mapping images and c) the corresponding elemental spectrum of CF@CoNC-4T.

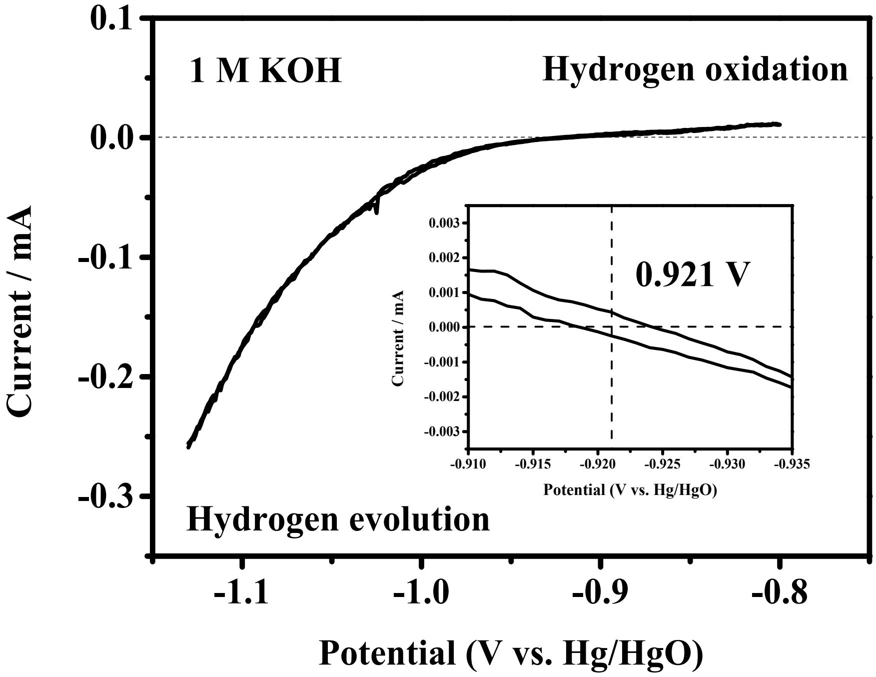

Figure S18. Single cycle CV curve of Hg/HgO electrode calibration in 1 M KOH at room temperature (~298 K).

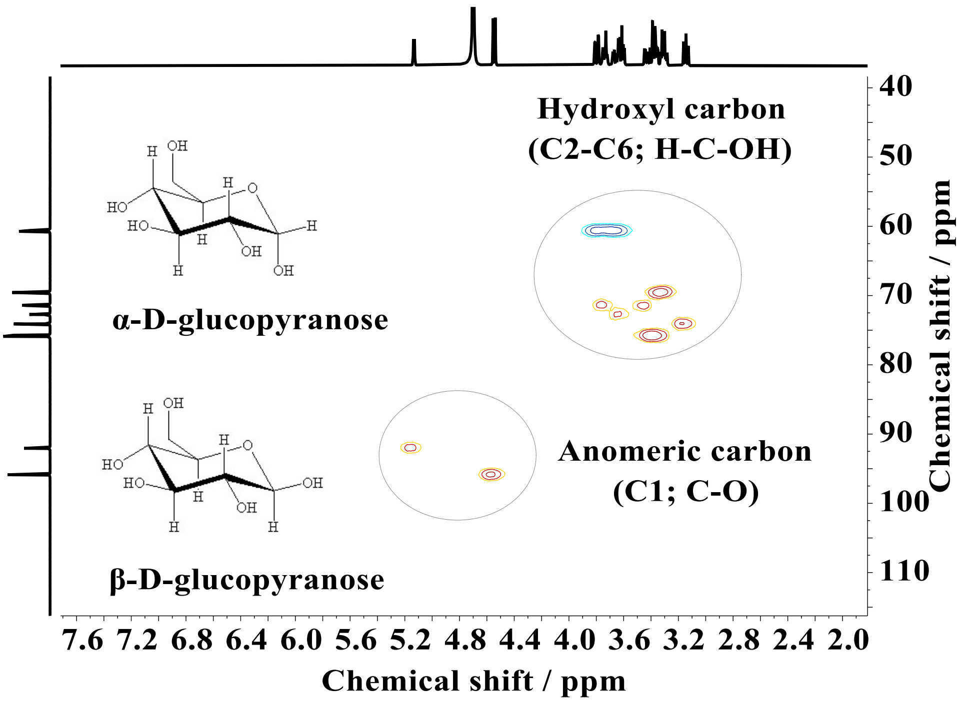

Figure S19. 2D HSQC NMR spectrum of pure D-glucose (absolute stereochemistry) in D_2O at 298 K.

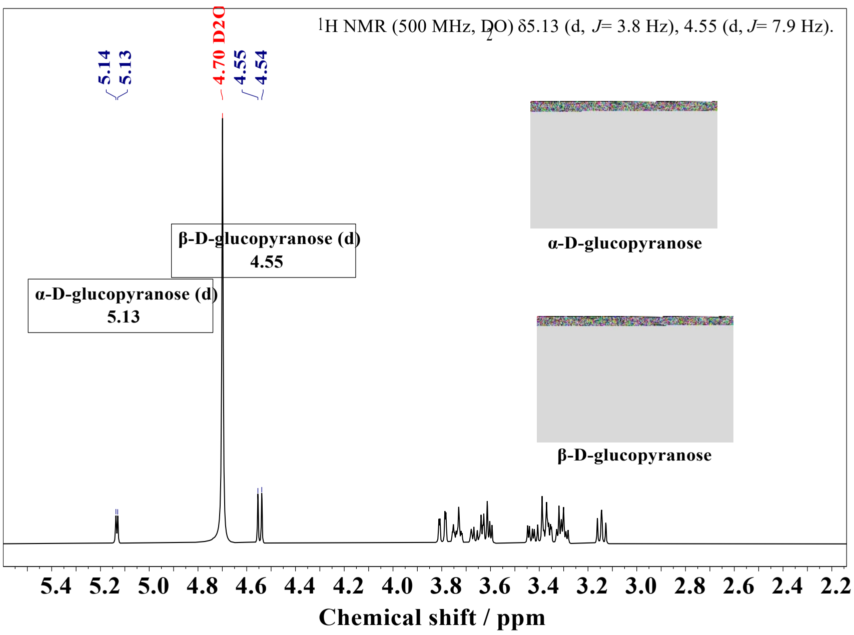

Figure S20. ^{1}H NMR (500 MHz) spectrum of pure D-glucose (absolute stereochemistry) in D_2O at 298 K.

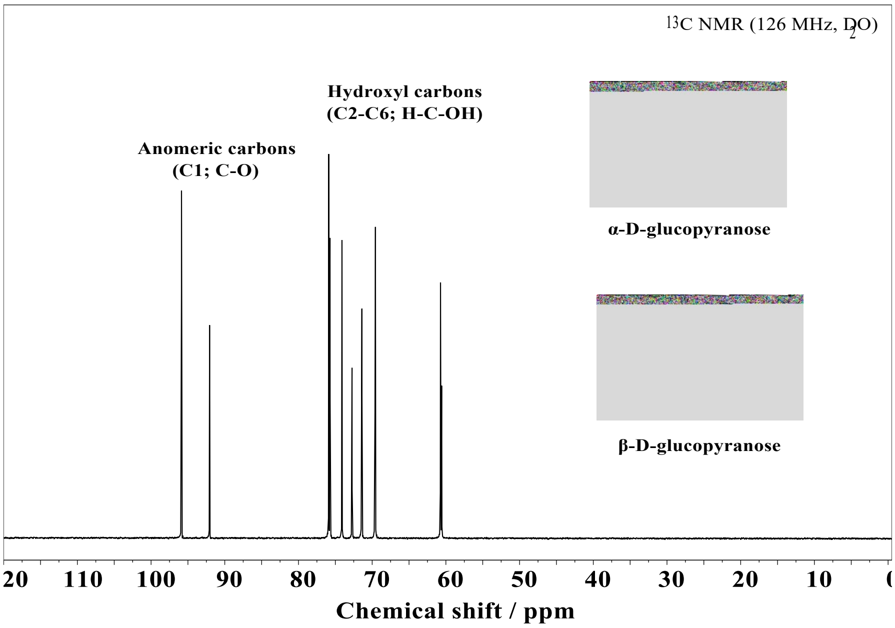

Figure S21. ^{13}C NMR (126 MHz) spectrum of pure D-glucose (absolute stereochemistry) in D_2O at 298 K.

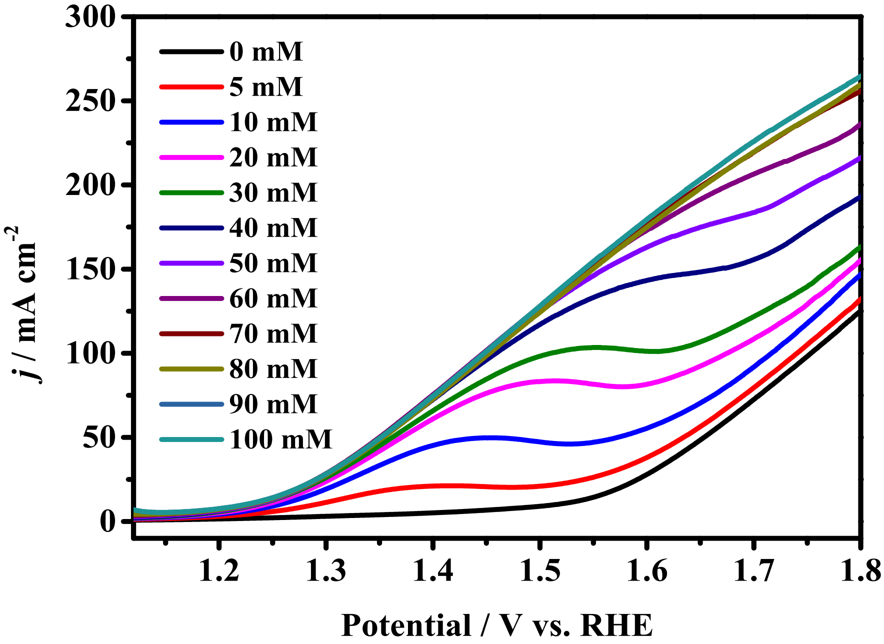

Figure S22. LSV curves of the CF@CoNC-1T electrode for glucose oxidation with different concentrations of glucose (0-100 mM).

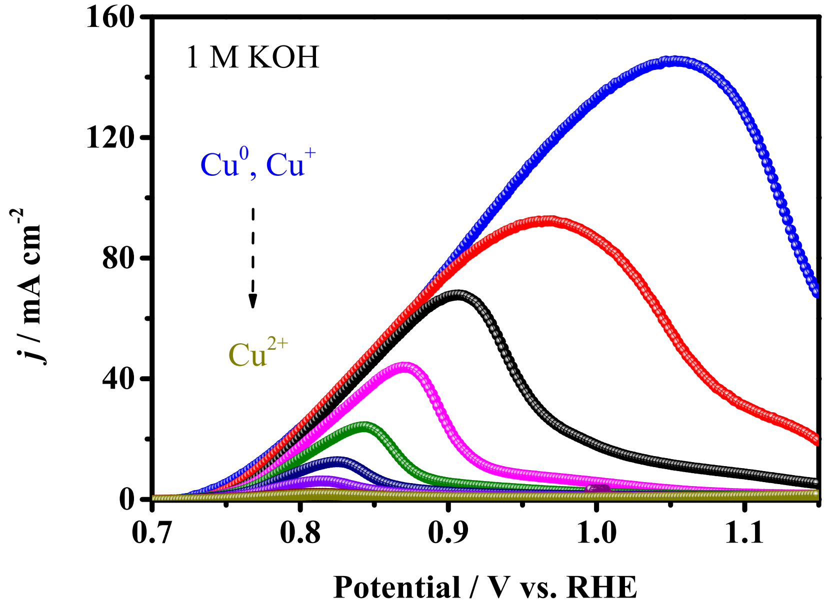

Fig. S23. LSV curves of the CF@CoNC-1T electrode in 1 M KOH. The oxidation peaks (Cu^0, $Cu^{1+} \rightarrow Cu^{2+}$) are gradually disappeared with multiple polarization curves scanning.

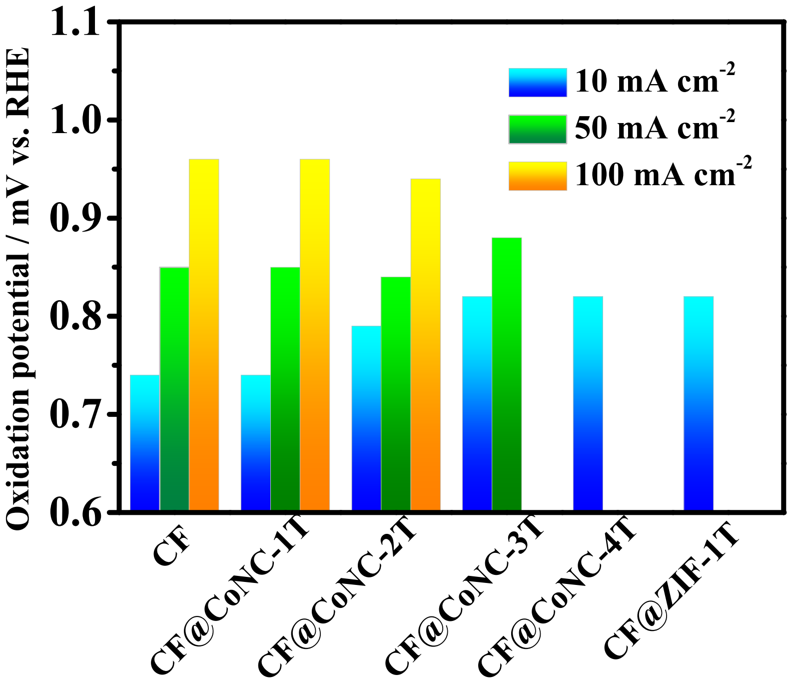

Figure S24. The copper oxidation potentials at different current densities for various electrocatalysts.

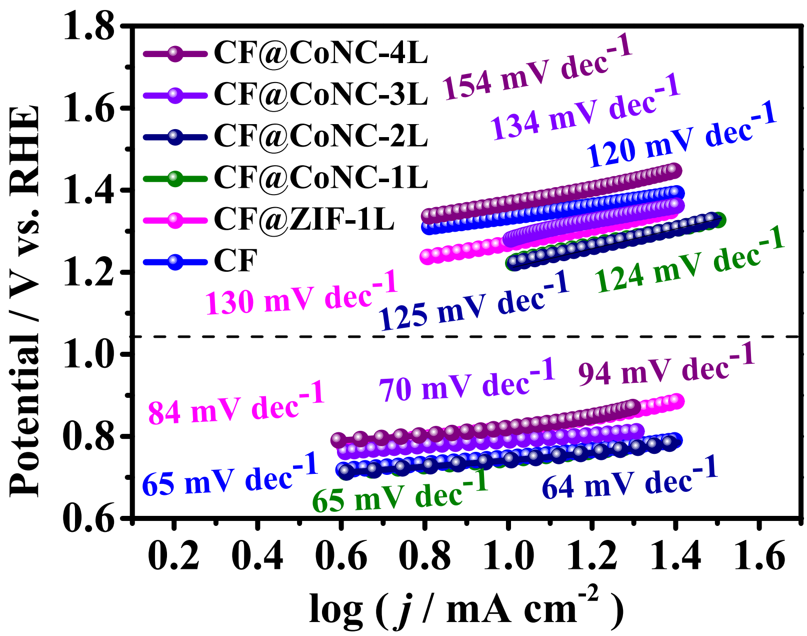

Figure S25. Tafel plots of copper foam (CF), CF@ZIF-1T and CF@CoNC-xT (x = 1-4) in copper oxidation and glucose oxidation reactions.

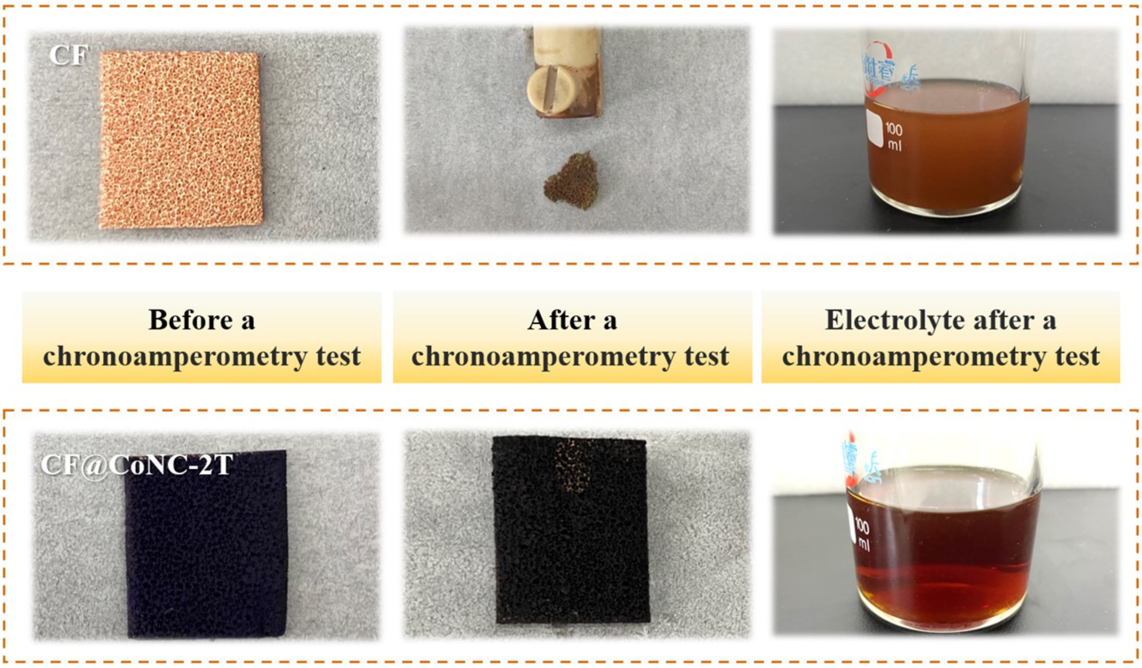

Figure S26. Optical images of the fresh and used CF and CF@CoNC and the used electrolyte solutions.

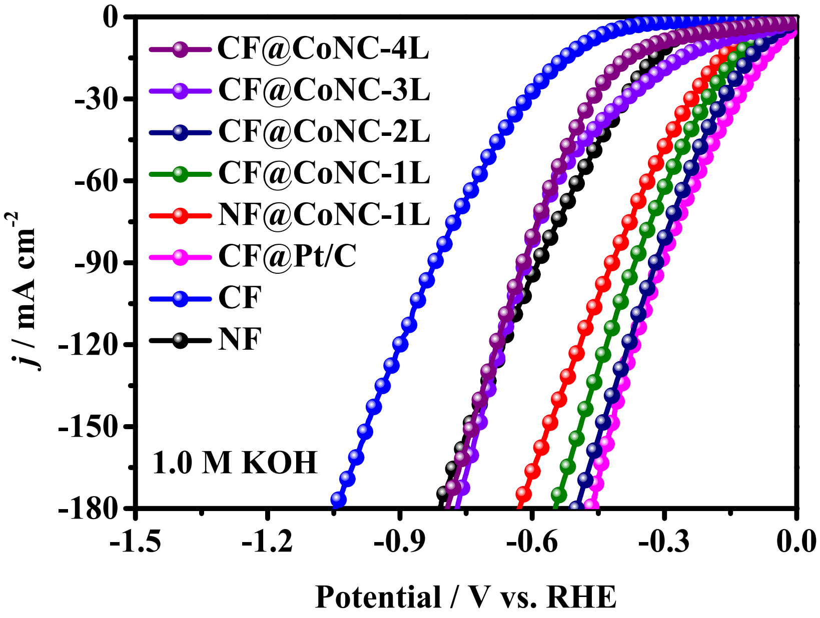

Figure S27. LSV curves of various electrocatalysts for HER without iR correction.

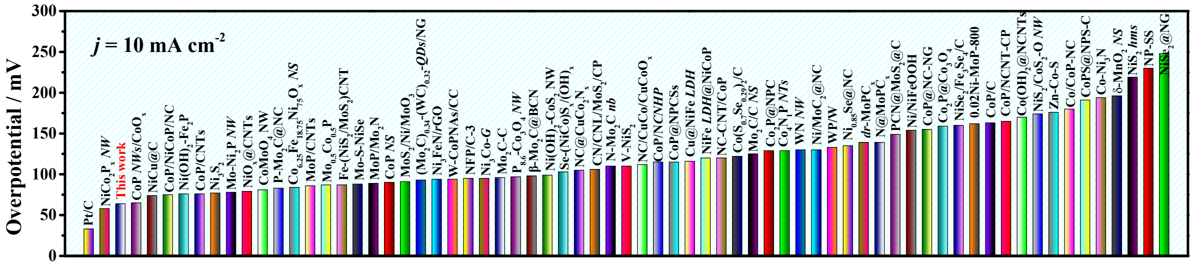

Figure S28. Comparison of the overpotential (j = 10 mA cm^{-2}) of our CF@CoNC-2T electrode with various previously reported HER electrocatalysts in 1 M KOH electrolyte.

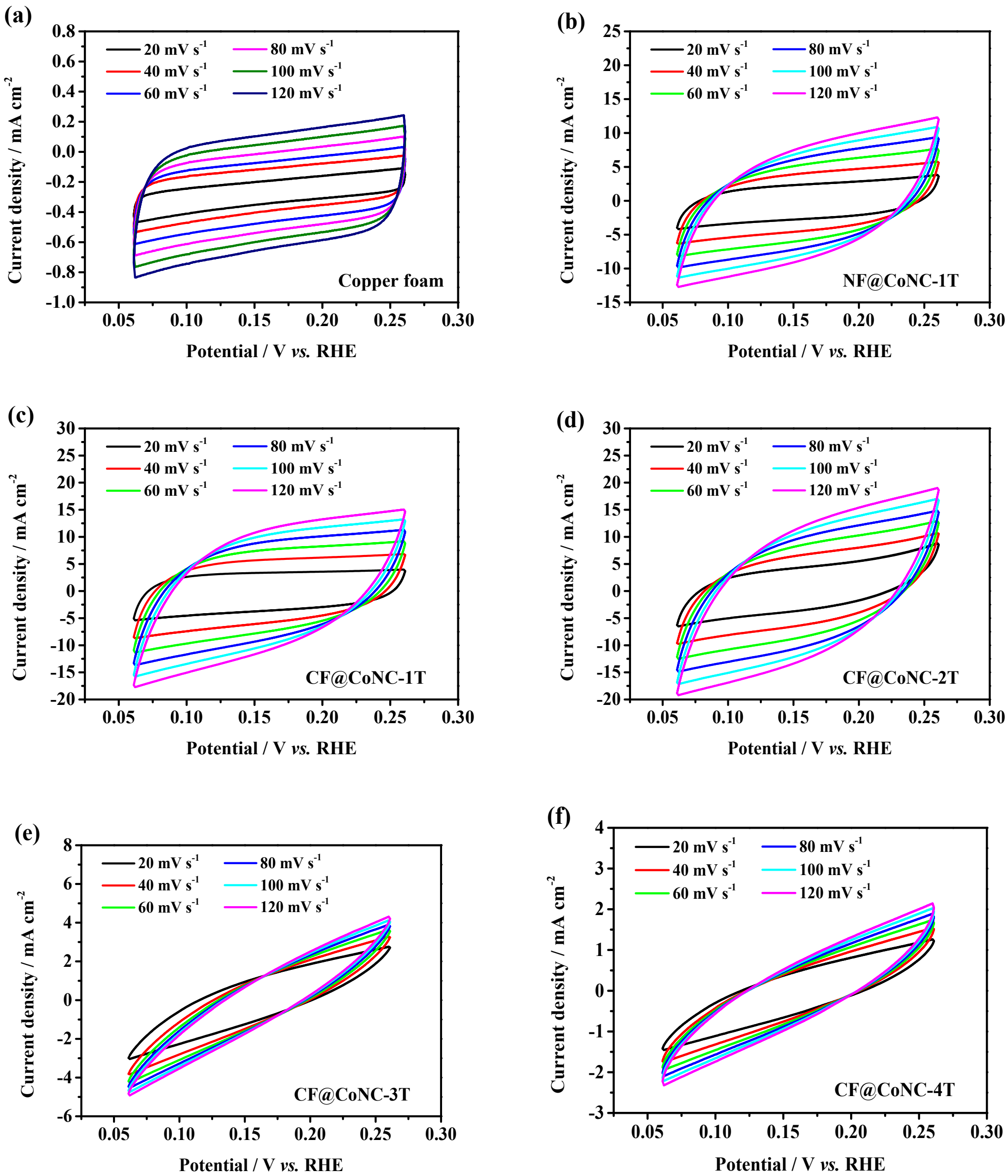

Figure S29. Cyclic voltammetry curves of (a) CF, (b) NF@CoNC-1T, (c) CF@CoNC-1T, (d) CF@CoNC-2T, (e) CF@CoNC-3T and (f) CF@CoNC-4T at different scan rates (20, 40, 60, 80, 100 and 120 mV s^{-1}) in 1.0 M KOH.

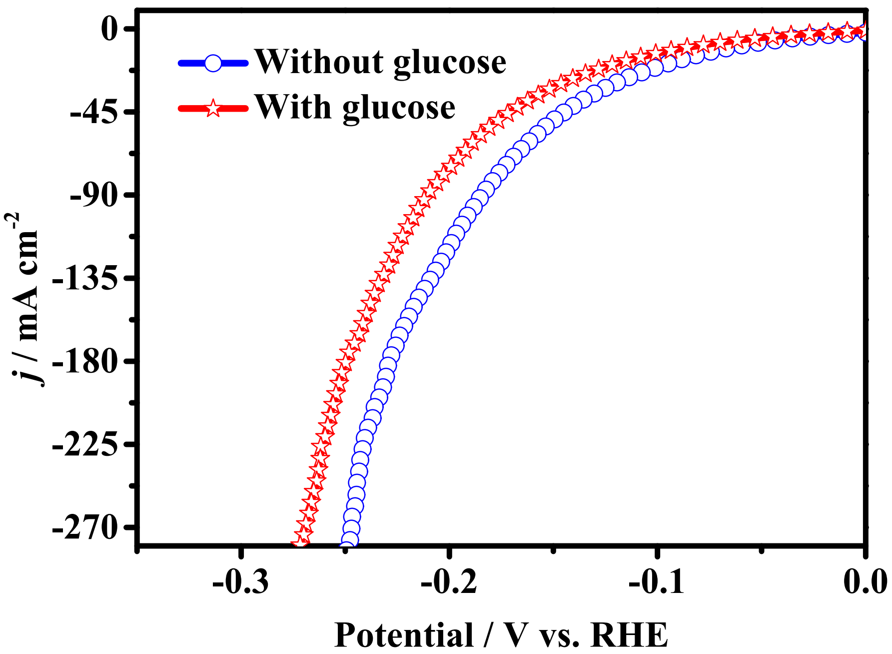

Figure S30. The LSV polarization curves of the CF@CoNC-2T electrode with and without100 mM glucose in HER.

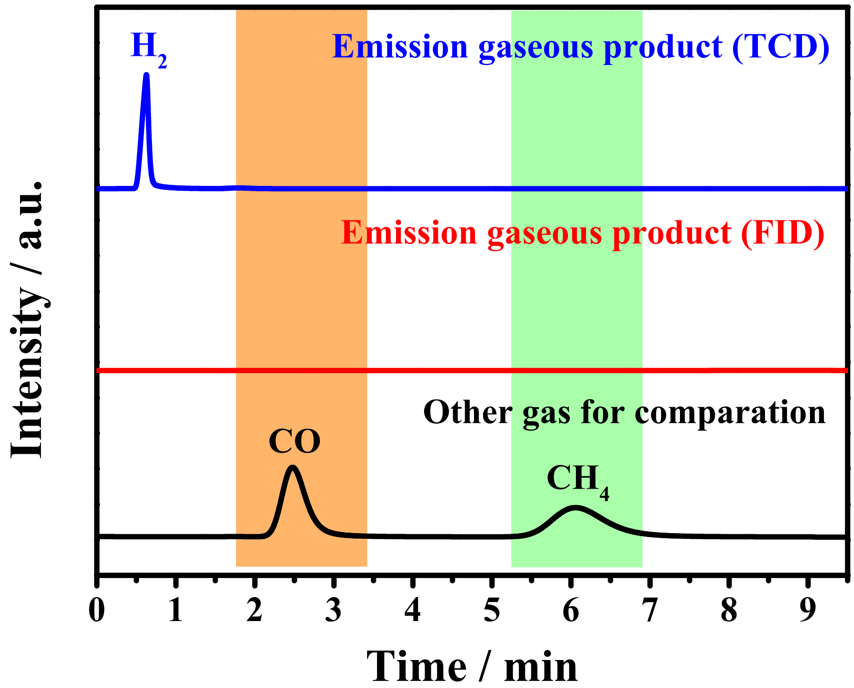

Figure S31. Analysis of emission gas by GC instrument.

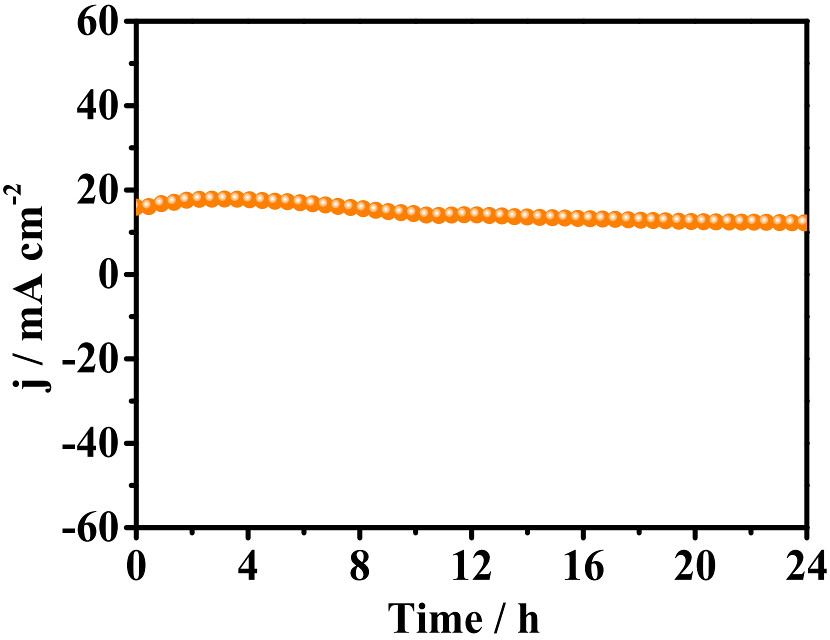

Figure S32. Long-term durability of the CF@CoNC-1T anode in a two-electrode system.

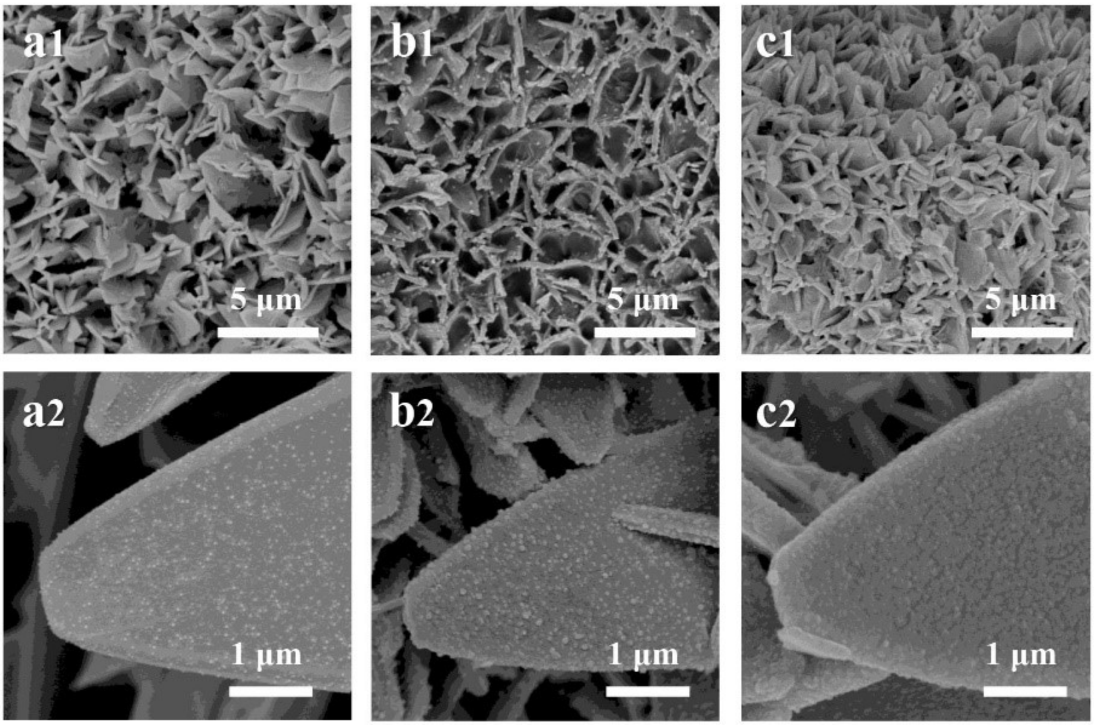

Figure S33. Low- and high-magnification SEM images of a) the fresh CF@CoNC-2T electrode, and b) the anodic CF@CoNC-2T and c) cathodic CF@CoNC-2T electrodes after the stability test.

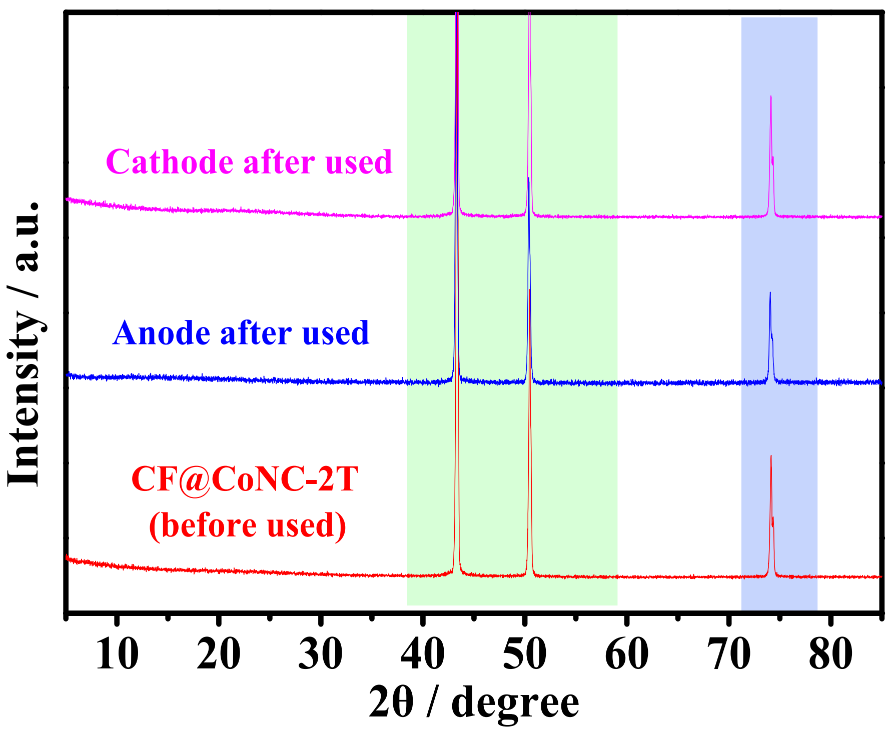

Figure S34. XRD patterns of CC@CoNC-600 electrode after used on cathode and anode.

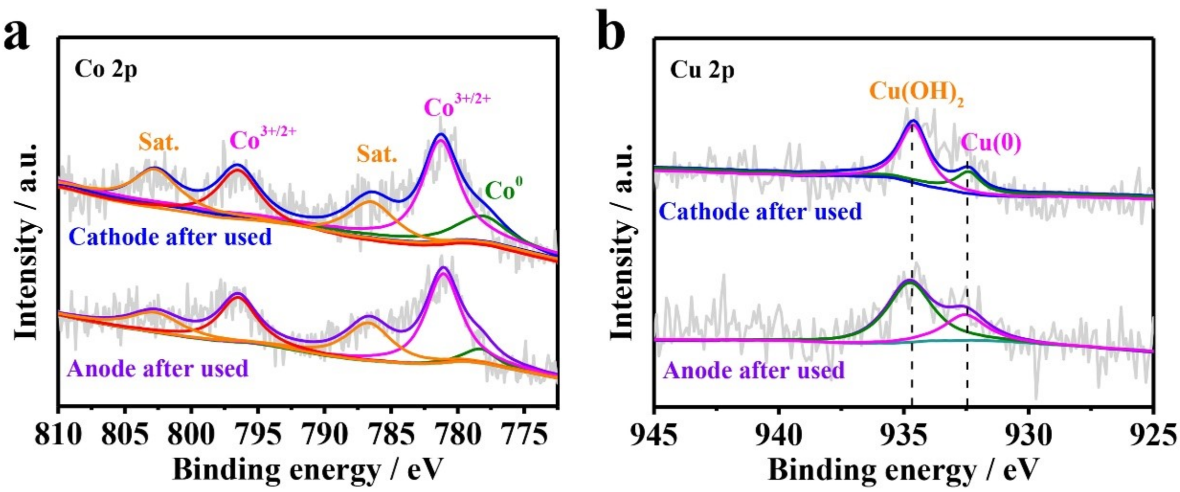

Figure S35. The high-resolution (a) Co 2p XPS spectra and (b) Cu 2p XPS spectra of CC@CoNC-2T electrode after used on cathode and anode.

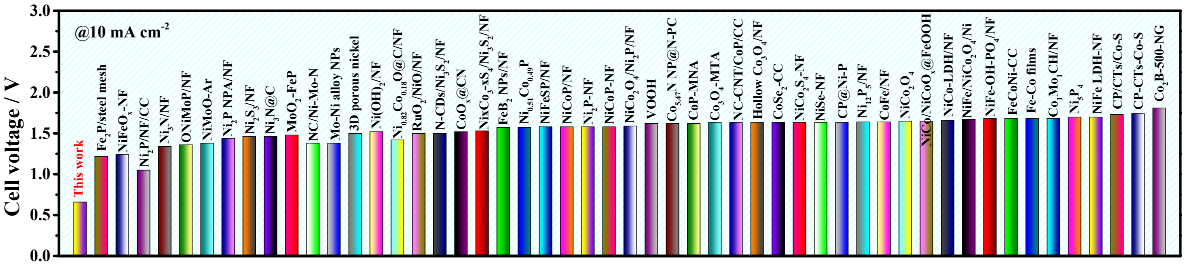

Figure S36. Comparison of the cell voltages of our system with some previously reported state-of-the-art electrocatalysts in overall water splitting H_2 production system.

Supplementary Tables

Table S1. Comparison of the element contents of CF, CF@ZIF-xT and CoNC-xT (x = 1-4) obtained from their SEM-EDS spectra.

Element /%	C	N	Co	Cu
CF@ZIF-1T	61.68	16.82	21.35	0.15
CF@ZIF-2T	58.26	35.54	6.10	0.10
CF@ZIF-3T	60.58	32.09	7.28	0.05
CF@ZIF-4T	58.12	35.13	6.74	0
CF@CoNC-1T	68.23	18.20	11.05	2.53
CF@CoNC-2T	51.39	2.39	45.45	0.78
CF@CoNC-3T	56.46	31.18	12.36	0
CF@CoNC-4T	56.13	33.11	10.75	0
CF	5.53	0.95	0	93.97

Table S2. Comparison of the HER performance of CF@CoNC-2T with various previously reported electrocatalysts in 1M KOH solution.

Catalysts	η@10 mA cm^{-2} / mV	References
CF@CoNC-2T	64	This work
Pt/C	33	Adv. Energy Mater., 2017, 8, 1701601
$NiCo_2P_x$ *NW*	58	Adv. Mater., 2017, 29, 1605502.
CoP *NWs*/CoO_x	65	Adv. Mater., 2018, 30, 1703322.
NiCu@C	74	Adv. Energy Mater., 2018, 8, 1701759
CoP/NiCoP/NC	75	Adv. Funct. Mater., 2019, 29, 1807976.
$Ni(OH)_2$-Fe_2P	76	Chem. Commun, 2018, 54, 1201-1204.
CoP/CNTs	76	Adv. Funct. Mater., 2017, 27, 1606635.
Ni_3S_2	77	ACS Appl. Mater. Interfaces, 2017, 9, 40162-40170
Mo-Ni_2P *NW*	78	Nanoscale, 2017, 9, 16674-16679
NiO_x@CNTs	79	ACS Appl. Mater. Interfaces, 2017, 9, 7139-7147.
$CoMoO_4$ *NW*	81	ACS Sustain. Chem. Eng, 2017, 5, 10093-10098.
P-Mo_2C@NC	83	Chem. Asian J, 2018, 13, 158-163.
$Co_{6.25}Fe_{18.75}Ni_{75}O_x$ *NS*	84	J. Mater. Chem. A, 2018, 6, 167-178.
MoP/CNTs	86	Adv. Funct. Mater, 2018, 28, 1706523.
$Ni_{0.5}Co_{0.5}P$	87	Electrochim. Acta, 2017, 249, 301-307.
Fe-(NiS_2/MoS_2)/CNT	87	J. Mater. Chem. A, 2020, 8, 17527-17536.
Mo-S-NiSe	88	J. Mater. Chem. A, 2017, 5, 20588-20593.
MoP/Mo_2N	89	Angew. Chem. Int. Ed., 2021, 133, 2-11.
CoP *NS*	90	New J. Chem, 2017, 41, 2436-2442.
MoS_2/NiS/MoO_3	91	ACS Appl. Mater. Interfaces, 2017, 9, 7084-7090.
$(Mo_2C)_{0.34}$-$(WC)_{0.32}$-*QDs*/N*G*	93	J. Mater. Chem. A, 2017, 5, 18494-18501.
Ni_3FeN/*rGO*	94	ACS Nano, 2018, 12, 245-253.
W-CoPNAs/CC	94	Small, 2019, 15, 1902613.

NFP/C-3	95	Sci. Adv., 2019, 5, eaav6009.
Ni_3Co-*G*	95	New J. Chem, 2017, 41, 5916-5923.
Mo_2C-C	96	J. Mater. Chem. A, 2017, 5, 4879-4885.
$P_{8.6}$-Co_3O_4 *NW*	97	ACS Catal, 2018, 8, 2236-2241.
β-Mo_2C@BCN	98	J. Mater. Chem. A, 2017, 5, 13122-13129.
$Ni(OH)_2$-CoS_2 *NW*	99	Nanoscale, 2017, 99, 16632-16637.
Se-$(NiCo)S_x/(OH)_x$	103	Adv. Mater, 2018, 30, 1705538.
NC@$CuCo_2N_x$	105	Adv. Funct. Mater, 2017, 27, 1704169.
CN/CNL/MoS_2/CP	106	Chem. Eng. J., 2012, 412, 128556.
N-Mo_2C *nb*	110	Appl. Catal. B, 2018, 224, 533-540.
V-NiS_2	110	ACS Nano, 2017, 11, 11574-11583.
NC/CuCo/$CuCoO_x$	112	Adv. Funct. Mater, 2018, 28, 1704447.
CoP/N*CNHP*	115	J. Am. Chem. Soc, 2018, 140, 2610-2618.
CoP@NPCSs	115	ACS Appl. Mater. Inter., 2018, 10, 51, 44201-44208.
Cu@NiFe *LDH*	116	Energy Environ. Sci, 2017, 10, 1820-1827.
NiFe *LDH*@NiCoP	120	Adv. Funct. Mater, 2018, 28, 1706847.
NC-CNT/CoP	120	J. Mater. Chem. A, 2018, 6,9009.
$Co(S_{0.71}Se_{0.29})_2$/C	122	Adv. Funct. Mater, 2017, 27, 1701008.
Mo_2C/C *NS*	125	ACS Appl. Mater. Interfaces, 2017, 9, 41314-41322.
Co_2P@NPC	129	Nanoscale, 2018, 10, 2902-2907.
Co_4Ni_1P *NTs*	129	Adv. Funct. Mater, 2017, 27, 1703455.
WN *NW*	130	J. Mater. Chem. A, 2017, 5, 19072-19078.
Ni/MoC_2@NC	130	Adv. Energy Mater, 2017, 7, 1700220.
WP/W	133	Chem. Eng. J, 2017, 327, 705-712.
$Ni_{0.85}Se$@NC	135	Small, 2020, 16, 2004231.
dr-MoN	139	J. Mater. Chem. A, 2017,5, 24193-24198.
N@$MoPC_x$	139	Adv. Energy Mater, 2017, 8, 1701601.
PCN@MoS_2@C	149	Chem. Commun., 2020, 56, 13393-13396.

Ni/NiFeOOH	154	ACS Appl. Mater. Interfaces, 2018, 10, 8585-8593.
CoP@NC-NG	155	Small, 2018, 14, 1702895.
Co_2P@Co_3O_4	159	J. Power Sources, 2018, 374, 142-148.
$NiSe_2/Fe_3Se_4/C$	160	J. Power Sources, 2017, 366,193-199.
0.02Ni–MoP-800	162	Nano Energy, 2020, 70, 104445.
CoP/C	163	J. Energy Chem, 2017, 26, 1147-1152.
CoP/NCNT-CP	165	ACS Sustainable Chem. Eng., 2019, 7, 10044-10051.
$Co(OH)_2$@NCNTs	170	Nano Energy, 2018, 47, 96-104.
NiS_2/CoS_2-O *NW*	174	Adv. Mater, 2017, 29, 1704681.
Zn-Co-S	176	Nanoscale, 2018, 10, 1774-1778.
Co/CoP-NC	180	Mater. Horiz, 2018, 5, 108-115.
CoPS@NPS-C	191	J. Mater. Chem. A, 2018, 6, 10433-10440.
Co-Ni_3N	194	Adv. Mater, 2018, 30, 1705516.
δ-MnO_2 *NS*	196	Adv. Energy Mater, 2017, 7, 1700005.
NiS_2 *hms*	219	J. Mater. Chem. A, 2017, 5, 20985-20992.
NP-*SS*	230	Adv. Mater., 2017, 29, 1702095
$NiSe_2$@NG	248	ACS Sustainable Chem. Eng., 2019, 7, 4351-4359.
Co_9S_8@NOSC	320	Adv. Funct. Mater., 2017, 17, 1606585.
NS-C	380	ACS Nano, 2017, 11, 7293-7300.

Table S3. Comparison of the required cell voltage and electricity consumption of our CF@CoNC-2T with several state-of-the-art noble-metal-free electrocatalysts for various organic-assisted electrocatalysis H_2 production systems.

Organic	Catalysts	Voltage / V 100 mA cm^{-2}	Electricity consumption / KWh m^{-3} H_2	References
Glucose	CF@CoNC-2T	0.90	1.97	This work
	$NiFeO_x$-NF	1.39	3.04	Nat. Commun. 2020, 11, 265.
	Fe_2P-films	1.58	3.46	Electrochem. Commun. 2017, 83, 11-15.
Urea	NiMoO-Ar	1.55	3.39	Energy Environ. Sci. 2018, 11, 1890-1897.
	ONiMoP/NF	1.68	3.68	Adv. Funct. Mater. 2021, 2104951.
	Ni_3N/NF	1.42	3.11	ACS Appl. Mater. Interfaces 2019, 11, 13168-13175.
	Ni_2P/NF	1.5	3.28	J. Mater. Chem. A 2017, 5, 3208-3213.
HMF	Ni_2S_3/NF	1.64	3.59	J. Am. Chem. Soc. 2016, 138, 13639-13646.
	Ni_3N@C	1.60	3.50	Angew. Chem. Int. Ed. 2019, 131, 16042-16050.
	Ni_2P	1.62	3.54	Angew. Chem. Int. Ed. 2016, 55, 9913-9917.
	MoO_2-FeP	1.66	3.63	Adv. Mater. 2020, 32, 2000455.
Alcohols	NC/Ni-Mo-N	1.60	3.50	Appl. Catal. B 2021, 298, 120493.
	3D porous Nickel	1.66	3.63	ACS Catal. 2017, 7, 4564-4570.
	Mo-Ni alloy NPs	1.53	3.35	J. Mater. Chem. A 2019, 7, 16501-16507.
	$Ni(OH)_2$/NF	1.66	3.63	Appl. Catal. B 2021, 281, 119510.

Table S4. Comparison of the required cell voltages of our CF@CoNC-2T at different current densities with various previously reported two-electrode organics-assisted electrocatalysis and overall water splitting H_2 production systems in 1M KOH solution.

Substrate	Electrode materials	Cell voltage / V			References
		10 mA cm^{-2}	50 mA cm^{-2}	100 mA cm^{-2}	
Glucose	CF@CoNC-2T (+) ‖ CF@CoNC-2T (-)	0.66	0.82	0.9	This work
		1.56 (H_2O)	1.72 (H_2O)	1.78 (H_2O)	
	Fe_2P/steel mesh (+) ‖ Pt/C (-)	1.22	1.50	1.58	Nat. Commun. 2020, 11, 265.
	$NiFeO_x$-NF (+) ‖ $NiFeN_x$/NF (-)	1.24	1.32	1.39	Electrochem. Commun. 2017, 83, 11-15.
Urea	Ni_2P/NF/CC (+) ‖ Ni_2P/NF/CC (-)	1.05	1.35	1.5	Energy Environ. Sci. 2018, 11, 1890-1897.
	Ni_3N/NF (+) ‖ Ni_3N/NF (-)	1.34	1.38	1.42	Adv. Funct. Mater. 2021, 2104951.
	ONiMoP/NF (+) ‖ ONiMoP/NF (-)	1.36	1.55	1.68	ACS Appl. Mater. Interfaces 2019, 11, 13168-13175.
	NiMoO-Ar (+) ‖ NiMoO-H_2 (-)	1.38	1.48	1.55	J. Mater. Chem. A 2017, 5, 3208-3213.
HMF	Ni_2P NPA/NF (+) ‖ Ni_2P NPA/NF (-)	1.44	1.58	1.62	J. Am. Chem. Soc. 2016, 138, 13639-13646.
	Ni_2S_3/NF (+) ‖ Ni_2S_3/NF (-)	1.46	1.58	1.64	Angew. Chem. Int. Ed. 2019, 131, 16042-16050.
	Ni_3N@C (+) ‖ Ni_3N@C (-)	1.46	1.55	1.60	Angew. Chem. Int. Ed. 2016, 55, 9913-9917.
	MoO_2-FeP (+) ‖ MoO_2-FeP (-)	1.48	1.59	1.66	Adv. Mater. 2020, 32, 2000455.
Alcohols	NC/Ni-Mo-N (+) ‖ NC/Ni-Mo-N (-)	1.38	1.47	1.60	Appl. Catal. B 2021, 298, 120493.
	Mo-Ni alloy NPs (+) ‖ Mo-Ni alloy NPs (-)	1.38	1.45	1.53	ACS Catal. 2017, 7, 4564-4570.
	3D porous nickel (+) ‖ 3D porous nickel (-)	1.50	1.60	1.66	J. Mater. Chem. A 2019, 7, 16501-16507.
	$Ni(OH)_2$/NF(+) ‖ $Ni(OH)_2$/NF (-)	1.52	1.62	1.66	Appl. Catal. B 2021, 281, 119510.

	$Ni_{0.82}Co_{0.18}O$@C/NF (+) || $Ni_{0.82}Co_{0.18}O$@C/NF (-)	1.42	\	\	Appl. Catal. B 2019, 252, 214-221.
	RuO_2/NiO/NF (+) || RuO_2/NiO/NF (-)	1.50	\	\	Small 2018, 14, 1704073.
	N-CDs/Ni_3S_2/NF (+) || N-CDs/Ni_3S_2/NF (-)	1.50	\	\	Carbon 2018, 129, 335-341.
	CoO_x@CN (+) || CoO_x@CN (-)	1.52	\	\	J. Am. Chem. Soc. 2015, 137, 2688-2694.
	$Ni_xCo_{3-x}S_4$/Ni_3S_2/NF (+) || $Ni_xCo_{3-x}S_4$/Ni_3S_2/NF (-)	1.53	1.68	1.80	Nano Energy 2017, 35, 161-170.
	FeB_2 NPs/NF (+) || FeB_2 NPs/NF (-)	1.57	\	\	Adv. Energy Mater. 2017, 7, 1700513.
	$Ni_{0.51}Co_{0.49}P$ (+) || $Ni_{0.51}Co_{0.49}P$ (-)	1.57	\	\	Adv. Funct. Mater. 2016, 26, 7644-7651.
	NiFeSP/NF (+) || NiFeSP/NF (-)	1.58	\	\	ACS Nano 2017, 11, 10303-10312.
	NiCoP/NF (+) || NiCoP/NF (-)	1.58	\	\	Nano Lett. 2016, 16, 7718-7725.
	Ni_2P-NF (+) || Ni_2P-NF (-)	1.58	\	\	ACS Catal. 2017, 7, 103-109.
H_2O	NiCoP-NF (+) || NiCoP-NF (-)	1.58	1.82	1.98	Nano Lett. 2016, 16, 7718-7725.
	$NiCo_2O_4$/Ni_2P/NF (+) || $NiCo_2O_4$/Ni_2P/NF (-)	1.59	\	\	Adv. Mater. Interfaces 2017, 4, 1700481.
	VOOH (+) || VOOH (-)	1.62	\	\	Angew. Chem. Int. Ed. 2017, 129, 588-592.
	$Co_{5.47}N$ NP@N-PC (+) || $Co_{5.47}N$ NP@N-PC (-)	1.62	\	\	ACS Appl. Mater. Interfaces 2018, 10, 7134-7144.
	CoP-MNA (+) || CoP-MNA (-)	1.62	\	\	Adv. Funct. Mater. 2015, 25, 7337-7347.
	Co_3O_4-MTA (+) || Co_3O_4-MTA (-)	1.63	\	\	Angew. Chem. Int. Ed. 2017, 56, 588-592.
	NC-CNT/CoP/CC (+) || NC-CNT/CoP/CC (-)	1.63	\	\	J. Mater. Chem. A 2018, 6, 9009-9018.
	Hollow Co_3O_4/NF (+) || Hollow Co_3O_4/NF (-)	1.63	\	\	Angew. Chem. Int. Ed. 2016, 56, 1324-1328.
	$CoSe_2$-CC (+) || $CoSe_2$-CC (-)	1.63	\	\	Adv. Mater. 2016, 28, 7527-7532.
	$NiCo_2S_4$-NF (+) ||	1.63	\	\	Adv. Funct. Mater.

	$NiCo_2S_4$-NF (-)				2016, 26, 4661-4672.
	NiSe-NF (+) ‖ NiSe-NF (-)	1.63	\	\	Angew. Chem. Int. Ed. 2015, 54, 9483-9487.
	CP@Ni-P (+) ‖ CP@Ni-P (-)	1.63	\	\	Adv. Funct. Mater. 2016, 26, 4067-4077.
	$Ni_{12}P_5$/NF (+) ‖ $Ni_{12}P_5$/NF (-)	1.64	\	\	ACS Catal. 2017, 7, 103-109.
	CoFe/NF (+) ‖ CoFe/NF (-)	1.64	\	\	Small 2018, 14, 1702568.
	$NiCo_2O_4$ (+) ‖ $NiCo_2O_4$ (-)	1.65	\	\	Angew. Chem. Int. Ed. 2016, 55, 1324-1328.
	NiCo/$NiCoO_x$@FeOOH (+) ‖ NiCo/$NiCoO_x$@FeOOH (-)	1.65	\	\	Electrochim. Acta 2017, 257, 1-8.
	NiCo-LDH/NF (+) ‖ NiCo-LDH/NF (-)	1.66	\	\	Dalton Trans. 2017, 46, 8372-8376.
	NiFe/$NiCo_2O_4$/Ni (+) ‖ NiFe/$NiCo_2O_4$/Ni (-)	1.67	\	\	Adv. Funct. Mater. 2016, 26, 3515-3523.
H_2O	NiFe-OH-PO_4/NF (+) ‖ NiFe-OH-PO_4/NF (-)	1.68	\	1.91	ACS Appl. Mater. Interfaces 2017, 9, 35837.
	FeCoNi-CC (+) ‖ FeCoNi-CC (-)	1.68	\	\	ACS Catal. 2017, 7, 469-479.
	Fe-Co films (+) ‖ Fe-Co films (-)	1.68	\	\	Nano Energy 2017, 38, 576-584.
	Co_1Mo_1CH/NF (+) ‖ Co_1Mo_1CH/NF (-)	1.68	\	\	J. Am. Chem. Soc. 2017, 139, 8320-8328.
	Ni_5P_4 (+) ‖ Ni_5P_4 (-)	1.70	\	\	Angew. Chem. Int. Ed. 2015, 54, 12361-12365.
	NiFe LDH-NF (+) ‖ NiFe LDH-NF (-)	1.70	\	\	Science 2014, 345, 1593-1596.
	CP/CTs/Co-S (+) ‖ CP/CTs/Co-S (-)	1.73	\	\	ACS Nano 2016, 10, 2342-2348.
	CP-CTs-Co-S (+) ‖ CP-CTs-Co-S (-)	1.74	\	\	ACS. Nano 2016, 10, 2342-2348.
	Co_2B-500-NG (+) ‖ Co_2B-500-NG (-)	1.81	\	\	Adv. Energy Mater. 2016, 6, 1502313.